Journal of Molecular and Cellular Cardiology 197 (2024) 20–33

Contents lists available at ScienceDirect

Journal of Molecular and Cellular Cardiology

journal homepage: www.elsevier.com/locate/yjmcc

Stochastic and alternating pacing paradigms to assess the stability of cardiac conduction

Stephan De Waard, Helene Hinnen, Jan P. Kucera *

Department of Physiology, University of Bern, Bühlplatz 5, CH-3012 Bern, Switzerland

ARTICLE INFO

Keywords:
Cardiac conduction
Conduction block
Current-to-load mismatch
Conduction stability
Mathematical modeling
Cardiomyocyte cultures

ABSTRACT

Reentry, the most common cause of severe arrhythmias, is initiated by slow conduction and conduction block. Hence, evaluating conduction velocity and conduction block is of primary importance. However, the assessment of cardiac conduction safety in experimental and clinical settings remains elusive. To identify markers of conduction instability that can be determined experimentally, we developed an approach based on new pacing paradigms. Conduction across a cardiac tissue expansion was assessed in computer simulations and in experiments using cultures of neonatal murine cardiomyocytes on microelectrode arrays. Simulated and in vitro tissues were paced at a progressively increasing rate, with stochastic or alternating variations of cycle length, until conduction block occurred. Increasing pacing rate led to conduction block near the expansion. When stochastic or alternating variations were introduced into the pacing protocol, the standard deviation and the amplitude of alternating variations of local conduction times emerged as markers of unstable conduction prone to block. In both simulations and experiments, conduction delays were prolonged at the expansion but increased only slightly during the pacing protocol. In contrast, these markers of instability increased several-fold, early before block occurrence. The first and second moments of these two metrics provided an estimation of the site of block and the accuracy of this estimation. Therefore, when beat-to-beat variations of pacing cycle length are introduced into a pacing protocol, the local variability of conduction permits to predict sites of block. Our pacing paradigms may have translational applications in clinical cardiac electrophysiology, particularly in identifying ablation targets during mapping procedures.

1. Introduction

The action potential (AP) is the electric signal that propagates through the heart to trigger the contraction of every myocyte [1]. Altered AP propagation can lead to arrhythmias. Most serious arrhythmias, such as fibrillation, are reentrant, whereby the same AP re-excites regions that have recovered from refractoriness [2]. Atrial fibrillation has a high prevalence [3,4], and by increasing the risk of heart failure and stroke, it is a major factor of morbidity and mortality [3,4]. Ventricular fibrillation leads to sudden circulatory arrest [5] and is fatal without immediate resuscitation measures [6].

Slow conduction and conduction block, especially unidirectional conduction block, are the key mechanisms of reentry initiation. Jointly, they permit the AP to re-excite the myocardium [2]. Hence, identifying situations where conduction velocity (CV) is altered and conduction is susceptible to block is of primary importance. Therefore, factors that determine and influence CV and block have been a central focus of research, with a particular emphasis on developing quantitative markers to describe the ability of an AP to propagate or not.

In mathematical modeling studies, the classical marker assessing AP propagation ability is the safety factor (SF) [7–12]. One definition of the SF was proposed by Shaw and Rudy [9] and subsequently refined by others [10,13]. Another definition of the SF was proposed by Boyle and Vigmond [11,12]. In these frameworks, the electric charge entering and exiting a given cell is compared to the capacitive charge required to depolarize the cell [9] or to the minimum charge required to produce an

Abbreviations: AP, Action potential; APD, Action potential duration; CL, Cycle length; CT, Conduction time between adjacent recording sites; CV, Conduction velocity; SD, Standard deviation; SD(CT), Standard deviation of CT in a sliding window of 10 APs; AA(CT), Amplitude of CT alternation in a sliding window of 10 APs; M_1, First moment (mean) of SD(CT) or AA(CT) considered as a distribution; M_2, Second moment (standard deviation) of SD(CT) or AA(CT) considered as a distribution; IBI, Interbeat interval; SD(IBI), Standard deviation of IBIs; AA(IBI), Amplitude of IBI alternation; MEA, Microelectrode array; SF, Safety factor.

* Corresponding author.
E-mail addresses: stephan.dewaard@unibe.ch (S. De Waard), helene.hinnen@unibe.ch (H. Hinnen), jan.kucera@unibe.ch (J.P. Kucera).

https://doi.org/10.1016/j.yjmcc.2024.10.007
Received 13 May 2024; Received in revised form 14 October 2024; Accepted 18 October 2024
Available online 20 October 2024

AP [11]. The interpretation of the SF is that the AP propagates if SF > 1, blocks if SF < 1, and is thus critical when SF = 1 [9,11].

However, real-world applications of the SF concept face a number of challenges. First, determining the SF requires the knowledge of currents and charges that, although being part of mathematical models, are not accessible directly in vitro or in vivo. Regarding the formulation by Shaw and Rudy [9], discrepancies at the critical limit between conduction and block and a value of SF = 1 were reported for conduction along a heterogeneous cell fiber [14]. The formulation by Shaw and Rudy was elaborated for 1-dimensional tissue (e.g., a cell fiber) and relies on the computation and integration of the current entering a given cell from upstream (I_{in}) and the current exiting that cell downstream (I_{out}) [9]. Identifying these currents is straightforward in one dimension. This formulation was subsequently used by Romero et al. [15,16], who refined the integration interval. However, in 2- or 3-dimensional tissue, a difficulty arises because I_{in} and I_{out} between adjacent simulation nodes are then influenced by the direction of propagation with respect to the discrete grid used for simulations [10]. Thus, applying the SF definition in 2 (or 3) dimensions requires to compute properly these currents. Accordingly, Romero et al. introduced an appropriate mathematical treatment of I_{in} and I_{out}, which permits to partially compensate the artefactual dependence of the SF on the direction of propagation [10]. Using their own SF definition, Vigmond and Boyle developed an elegant approach based on second spatial derivatives [12] to estimate transmembrane currents densities using recordings with extracellular electrodes. However, this estimation requires assumptions regarding extracellular conductivity, and experiments must then be conducted additionally to determine threshold currents that lead to APs in isolated cells. Despite these challenges, because conduction block is a crucial arrhythmogenic mechanism, efforts should be maintained to develop quantitative markers that could ideally also be obtained experimentally. Such efforts bear promise for the development and refinement of strategies to prevent and treat, e.g., atrial or ventricular fibrillation using catheter ablation.

In the present study, we propose a new paradigm to evaluate the stability of conduction and to identify sites where conduction is prone to block. Our main hypothesis is that a decrease in stability (before block occurs) is accompanied by an increased response to perturbations, especially at locations where depolarization reserve is already critical. Such an increased response could then be interpreted as a warning that block is imminent. In paced cardiac tissue, a straightforward way to perturb AP propagation in a controlled manner is to modify the pacing interval (e.g., using a S1S2 protocol [17]). If the pacing interval is shortened such that the stimulus lies in the relative refractory period, the recovery of the Na^+ current is incomplete. Consequently, this engages the restitution of CV and depresses the stability of conduction. Here, we combined consecutive variations of pacing intervals, i.e. randomly varying intervals and alternating intervals. We hypothesized that these repeated perturbations would result in measurable variations of the excitation pattern, thus permitting to identify sites of unstable conduction most prone to block.

We implemented this approach in a mathematical model of conduction and in patterned cardiac cell cultures grown on microelectrode arrays. We considered conduction across an expansion of cardiac tissue, a stereotypical structure known to exhibit current source-to-load mismatch and susceptibility to block [2,11,12,18–20]. When beat-to-beat variations of pacing cycle length (CL) were introduced, analyzing the variations of local conduction times (CTs) over consecutive impulses permitted to derive markers of conduction instability and to anticipate the location of conduction block. Our proof-of-principle study may thus open avenues in clinical mapping studies for non-conventional pacing protocols to yield diagnostic and prognostic markers to identify sites prone to block.

2. Materials and methods

Detailed materials and methods are provided as Supplementary material.

2.1. Modeling of conduction across expansions

2.1.1. Model of an expanding strand in 2 dimensions

Conduction was simulated in a 2-dimensional network representing a rectangular expansion of cardiac tissue, as illustrated in Fig. 1A and as used in previous work [21]. The computational domain consisted of a 2-dimensional network of excitable elements arranged on a square lattice, with a discretization (element size) of $\Delta x = \Delta y = 60$ μm. Unless specified otherwise, the network consisted of a 5-element wide and 50-element long strand (i.e., 300 μm wide and 3 mm long), merging into a 50-element by 101-element (3 by 6.06 mm) rectangular expansion (Fig. 1A). For the ion currents, we used a modified version of the Luo-Rudy 1 model [22] that was adjusted to replicate previous observations in small rodent cardiomyocyte cultures [21,23–25]. Coupling between the excitable nodes was homogeneous and isotropic. Details of the model are presented in the Supplementary material. The model tissue was paced at the extremity of the strand (see Fig. 1A) by injecting a 2-ms suprathreshold depolarizing current pulse into the first column of excitable elements or, for simulations of retrograde conduction, into the last column of elements along the right edge of the network. Membrane potential was registered at 10 locations evenly spaced (300 μm) along the axis of the strand (Fig. 1A). Activation time was defined at these locations as the moment when membrane potential passed −35 mV during depolarization. These activation times were used to calculate the successive conduction times (CTs) between adjacent recording locations. These CTs were subsequently analyzed in a similar manner as for the in vitro experiments to compute metrics assessing conduction stability (see section 2.3.2 below).

2.1.2. Pacing protocols

Three different types of protocols were implemented. Similar pacing protocols were used in simulations and in vitro experiments.

2.1.3. Ramp protocol without variations

After an initial 6 s period at a predefined basic cycle length (200–250 ms), the CL was progressively decreased (Fig. 1B, top left panel) on a beat-to-beat basis to 80–100 ms over several minutes, which ultimately led to the occurrence of conduction block at the expansion site. The ramps were constructed such that the instantaneous pacing rate (1/CL) rather than CL itself changed linearly with time (Fig. 1B, bottom left panel), as done previously [26].

2.1.4. Ramp protocol with stochastic variations

A sequence of pacing CLs was constructed as described above. Then, every CL was perturbed by adding a random number from a Gaussian distribution with zero mean and a standard deviation (SD) of either 2 or 5 ms.

Ramp protocol with alternating variations: The even terms of the CL series without variations were lengthened by 2 or 5 ms and the odd terms were shortened by the same amount.

All simulations were run in MATLAB (version R2019a, MathWorks).

2.2. Experiments in patterned cardiomyocyte cultures grown on microelectrode arrays

2.2.1. Patterned cultures on microelectrode arrays

Patterned cardiomyocyte cultures derived from neonatal (0–1 day postpartum) or fetal (19.5 days postcoitum) wild-type C57BL/6 J mice (Charles River) were prepared as described previously [23,27–29]. The myocytes were seeded (density: 4.4×10^5 cells/cm^2) on microelectrode arrays (MEAs; Campus Biotech, Geneva, Switzerland) that were

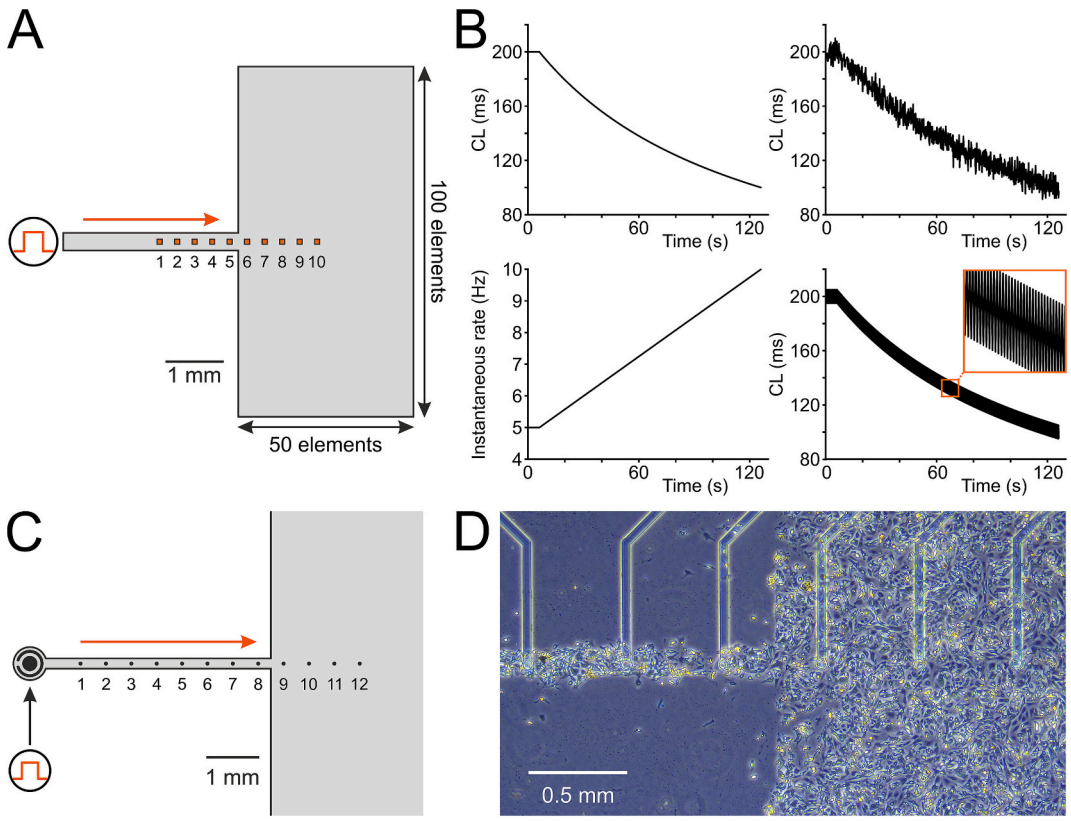

Fig. 1. New pacing paradigms to evaluate conduction stability in silico and in vitro. A: Schematic of the computational domain consisting of a strand merging into a rectangular expansion. The orange arrow denotes the direction of propagation, which is prone to be blocked by the current-to-load mismatch. The numbered orange squares indicate the excitable elements at which membrane potentials were registered. B: *Top left:* Ramp pacing protocol without variations. *Bottom left:* Same protocol represented as instantaneous rate vs. time. *Top right:* Ramp protocol with stochastic beat-to-beat variations with a SD of 5 ms. *Bottom right:* Ramp protocol with alternating ±5 ms variations (see inset). C: Schematic (grey) of a patterned cardiomyocyte culture grown over a row of 12 electrodes (numbered black dots). The black structure on the left represents the stimulation dipole. The orange arrow denotes the direction of propagation. D: Phase-contrast microphotograph of a preparation showing the cell strand merging into the expansion and the neighboring 6 electrodes (visible as small circles) and leads.

mounted in custom culture chambers [20]. The MEAs incorporated four rows of 12 recording electrodes (diameter: 40 μm; spacing: 0.5 mm) with a platinized stimulation dipole at each end (Fig. 1C). Over these rows of electrodes, cardiomyocyte strands (width: 100–150 μm) expanding abruptly into rectangular expansions were patterned using a photolithographic technique [30]. The preparations were incubated at 36 °C and 0.9 % CO_2 for 2–3 days prior to experiments. A schematic and a microphotograph of a preparation are shown in Fig. 1D.

All procedures were performed in compliance with ethical principles and guidelines set forth by the Swiss Academy of Medical Sciences. The protocols were approved by the Commission of Animal Experimentation of the Cantonal Veterinary Office of the Canton of Bern, Switzerland, in accordance with Swiss legislation.

2.2.2. Electrophysiological recordings

For electrophysiological experiments, the culture medium was replaced with Hanks' balanced salts solution (Gibco). The chambers, which incorporated a connection interface, were linked to a custom amplifier array (gain: 1000 x) and stimulator, and replaced into the incubator (36 °C) for an equilibration period of ~60 min.

The preparations were stimulated using biphasic voltage pulses (amplitude 0.7–1.5 V, duration 1 ms). For every expansion investigated, a ramp protocol without variations, two ramp protocols with stochastic CL variations (SD of 2 ms and 5 ms) and two ramp protocols with alternating CL variations (± 2 ms and ± 5 ms) were conducted (see Fig. 1B). Only preparations demonstrating continuous 1:1 stimulus capture (before block eventually occurred at the expansion) were used for further analysis. Extracellular unipolar electrograms were sampled at 10 kHz.

2.3. Data analysis: metrics to assess conduction instability

2.3.1. Conduction times in the experimental recordings

The electrograms were high-pass filtered using a digital AC coupling filter (time constant: 1 ms) to decrease the capacitive transients consecutive to the stimulation artifacts. Then, in a first step, activation times were identified at the occurrence of the minimum of the first derivative [20,23]. All electrograms were curated by visual inspection using a custom-designed graphic user interface to ensure that all activations were detected properly. In a second step, we used the algorithm of Shors et al. [31] to have a precise determination of CTs between adjacent electrodes. This algorithm is resilient to noise and provides stable results with an accuracy in the range of 5 % of the sampling period [31]. The signals from the two electrodes most proximal to the stimulation site were strongly distorted by the stimulation artifacts and were thus not considered, leaving 10 electrodes with 9 equally spaced intervals. This analysis was conducted until the first occurrence of block at the expansion site (confirmed by visual inspection of the signals).

2.3.2. Metrics to assess conduction stability

In simulations and experiments, for every interval between adjacent recording locations, we computed the standard deviation of CTs (SD (CT)) and the amplitude of alternating variations of CTs (AA(CT)) in a sliding window of 10 consecutive APs. SD(CT) was used to examine the variability of conduction during ramps with stochastic variations. AA (CT) was used to examine the variability of conduction during ramps

with alternating variations and was computed as the absolute difference between the mean of the odd values and the mean of the even values within the sliding window. For these computations, the sequence of 10 consecutive CT values was detrended using a second-degree polynomial.

In selected simulations, the safety factor was computed according to the SF_{m2} formulation by Romero et al. [10].

2.3.3. Metrics to predict the site of block in experiments

To evaluate the ability of SD(CT) and AA(CT) to localize sites of conduction prone to block, their corresponding values were considered as a distribution over the interelectrode intervals, and their first two moments were calculated. The first moment M_1 corresponds to the location of the mean of the distribution and provides an estimate of the site of block. The square root M_2 of the second moment (centered on M_1) corresponds to the standard deviation of the distribution and is a measure of the accuracy of this estimation. All analyses were done in MATLAB.

3. Results

3.1. Computer simulations identify SD(CT) and AA(CT) as predictive markers for the occurrence and localization of conduction block

In a first step, we ran computer simulations using pacing ramps with stochastic or alternating variations of CL to examine whether the standard deviation of conduction times (SD(CT)) and the amplitude of CT alternations (AA(CT)) may be suitable markers for the occurrence and localization of block across a tissue expansion. The simulation setup is illustrated in Fig. 2A, where the 9 intervals between the recording sites are color-coded. The left panel of Fig. 2B shows transmembrane AP upstrokes reflecting successful AP propagation at the beginning of a control ramp without variations (shown in Fig. 2C). Because of the current-to-load mismatch, the upstrokes were distorted, and conduction exhibited a local delay around the expansion site. The distortion of the AP upstrokes near the expansion is due to the bidirectional electrotonic interactions across the expansion site. Typically, as the wavefront progresses into the expansion, biphasic “double-hump” upstrokes appear, with a primary upstroke followed by a secondary one. The first upstroke is influenced by the magnitude of the electrical load exerted by the expansion, and the secondary upstroke results from the progressive decrease of this electrical load as distal tissue depolarizes. These typical changes in AP upstroke morphology have been previously described in detail (e.g., [19,32]). The right panel of Fig. 2B shows membrane potentials for the first impulse that was blocked by the expansion, characterized by upstrokes of decreasing amplitude and the absence of depolarization at distal sites. This first block occurred after 113 s during the ramp protocol at a CL of 126 ms. Thereafter, block exhibited a 2:1 pattern (not shown).

The bottom plots of Fig. 2C show the evolution of CT and SD(CT) (over a sliding window of 10 previous impulses) during the 50 s that preceded the first occurrence of block. CT was longer for intervals #5 and #6 (at the expansion and just after it), with a sharp increase for interval #6 in the last seconds preceding block. However, SD(CT) remained near 0 and rose to 0.2 ms (for interval #6) only for the last few impulses before block. Fig. 2D and E show the same analysis as in Fig. 2C, but for pacing protocols to which stochastic variations with a SD of 2 ms or 5 ms were added, respectively. Compared to the ramp without variations, the first block occurred earlier (after 108 s with a SD of 2 ms, after 87 s with a SD of 5 ms), but at a similar CL (125 ms and 124 ms). As a consequence of the earlier occurrence of block due to the stochastic variations, the CTs increased only mildly but exhibited prominent beat-to-beat variations for intervals #5 and #6. Importantly, when quantified by SD(CT), these variations were larger for intervals #5 and #6 than for the other intervals. This difference was already apparent 50 s before block occurred, and SD(CT) increased several-fold during the last 25 s before block. These results suggest that SD(CT) is an appropriate marker to anticipate the localization and occurrence of conduction block. These observations are in line with our hypothesis that unstable conduction near the expansion can be revealed by introducing perturbations, here in the form of random CL variations.

We then investigated pacing protocols with alternating variations of CL and the corresponding metric AA(CT), evaluated over a sliding window of 10 impulses. Fig. 2F shows that in the absence of alternating variations (same pacing protocol as in Fig. 2C), AA(CT) remained 0 except for the last few impulses before block. Similar to stochastic variations, alternating CL variations of ± 2 ms (Fig. 2G) and ± 5 ms (Fig. 2H) led to earlier occurrence of block (after 110 and 103 s, respectively, compared to 113 s in the absence of variations), albeit at the same CL (125 ms). Notably, alternating CL variations led to manifest alternation of CT for intervals #5 and #6 (insets), reflected by the many-fold increase of AA(CT) for these two intervals already tens of seconds before the first block. In addition, AA(CT) was larger for these two intervals compared to the other intervals already 50 s before block occurred. These results therefore indicate that unstable conduction can also be detected using alternating perturbations of CL.

Noteworthy, the increased SD(CT) and AA(CT) near the expansion reflected a critical and unstable depolarization reserve. As illustrated by Supplemental Fig. S1 showing model variables at the beginning of pacing and at the moment of block, this critical and unstable reserve resulted from the stimuli being applied during the steeper phase of the diastolic recovery of the sodium current from inactivation.

As a negative control, we conducted the same computational analysis for retrograde AP propagation, i.e. for the same domain paced along the right edge of the rectangular expansion (Supplemental Fig. S2A). Because of the absence of current source-to-load mismatch, no major distortion of the AP upstroke was observed across the expansion-strand boundary, and propagation eventually failed at the stimulation site (Supplemental Fig. S2B). As opposed to antegrade conduction, CT and SD(CT) did not manifestly increase with CL shortening near the region of the expansion during retrograde conduction when control ramps and ramps with stochastic variations were applied (Supplemental Figs. S2C, S2D and S2E). When ramps with alternating variations were applied, CT and AA(CT) did not increase either (Supplemental Figs. S2F, S2G and S2H). Hence, tissue expansions were prone to blocks that were unidirectional and they were not sensitive to pacing perturbations during retrograde conduction.

Overall, in contrast to the ramp without variations, stochastic and alternating pacing allow to derive markers of conduction stability and to anticipate the occurrence and localization of conduction block, with SD (CT) and AA(CT) exhibiting a considerably larger increase than CT itself.

3.2. In vitro experiments confirm SD(CT) and AA(CT) as predictive markers for the occurrence and the localization of conduction block

To challenge the model findings in an experimental setting, we assessed conduction across a tissue expansion in patterned cultures of mouse neonatal ventricular cardiomyocytes using microelectrode arrays. Fig. 3 presents results from a representative experiment. A schematic of the preparation is illustrated in Fig. 3A. The preparation was paced by the dipole on the left and the nine color-coded intervals between adjacent recording electrodes were used to calculate CTs. Similar to computer simulations, conduction stability was evaluated using a ramp protocol starting with a CL of 200 ms and progressively decreasing to a CL of 80 ms (Fig. 3B). Fig. 3C shows the recorded electrograms during successful impulse propagation at the beginning of the pacing protocol (a, green dot on the ramp depicted in Fig. 3B) and for the first impulse that was blocked at the expansion site (b, red dot in Fig. 3B).

As for the simulations, we compared the results yielded by the pacing protocol without variations (control protocol, Fig. 3D) to those obtained with stochastic variations (SD of 5 ms, Fig. 3E) and with alternating variations (± 5 ms, Fig. 3F). Without CL variations, the first conduction block occurred in the interval bridging the expansion site after 125 s, at a

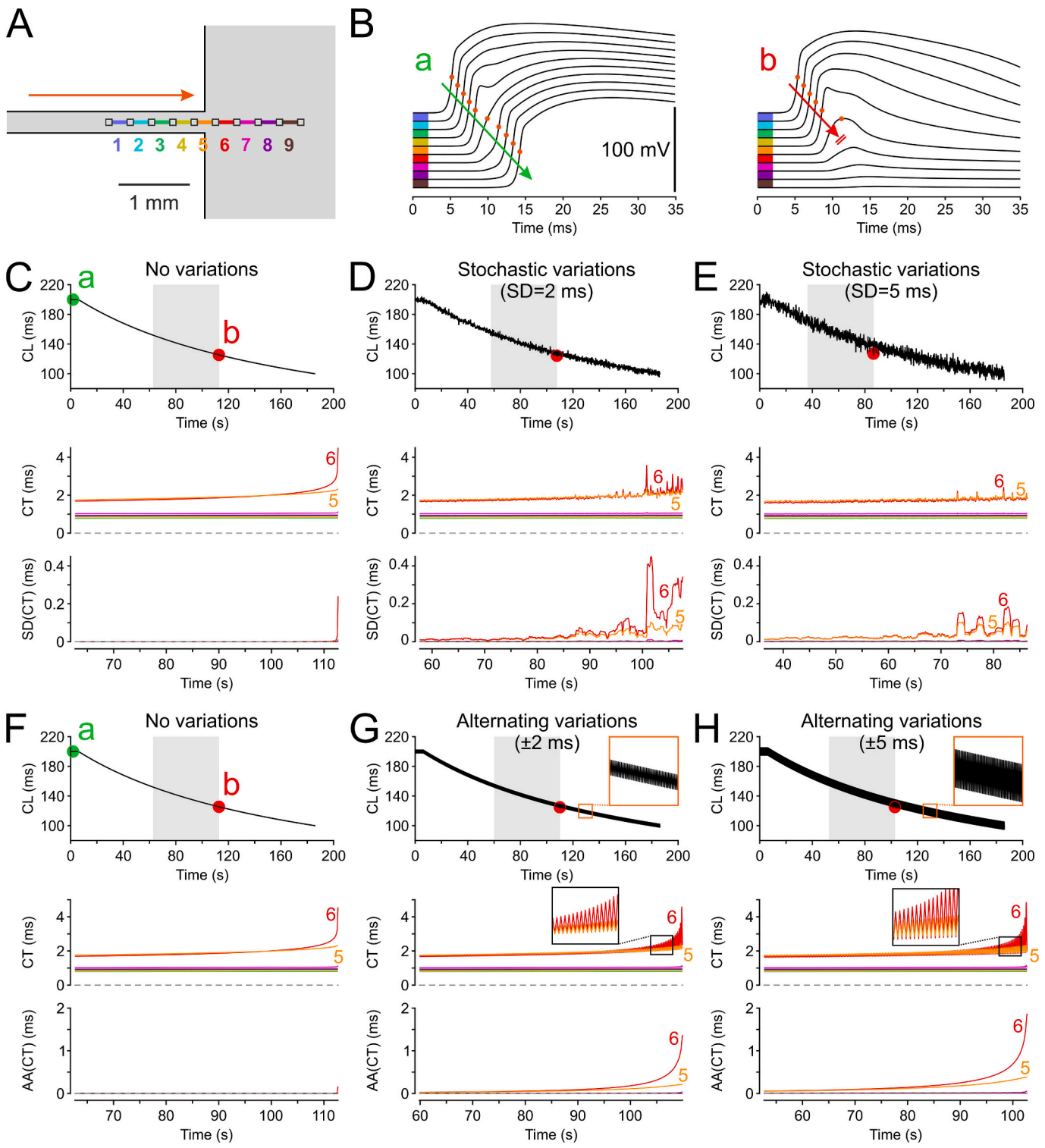

Fig. 2. Simulations of conduction variability across a tissue expansion. A: Schematic of the computational domain, with numbered and color-coded intervals between recording sites. B: Membrane potentials at the sites marked in A for a successfully propagated impulse at the beginning of a control pacing ramp (a, green arrow) and for the first impulse that was blocked by the expansion (b, red arrow). Color coding as in A. The orange dots indicate the threshold of −35 mV defining activation time. C: *Top:* Ramp protocol without variations. The green and red markers correspond to the upstrokes shown in B. *Middle and bottom:* CT and SD(CT) during the last 50 s before block (grey background in the ramp protocol). Labeling and color-coding as in A. D and E: Same as C, but for a ramp protocol with stochastic CL variations having a SD of 2 ms and 5 ms, respectively. The red marker indicates the first impulse blocked at the expansion. F: *Top:* Ramp protocol without variations (as in C). *Middle and bottom:* CT and AA(CT) during the last 50 s before block (grey background in the ramp protocol). G and H: Same as F, but for a ramp protocol with alternating CL variations of ± 2 ms and ± 5 ms, respectively. The red marker indicates the first impulse blocked by the expansion. (For interpretation of the references to color in this figure legend, the reader is referred to the web version of this article.)

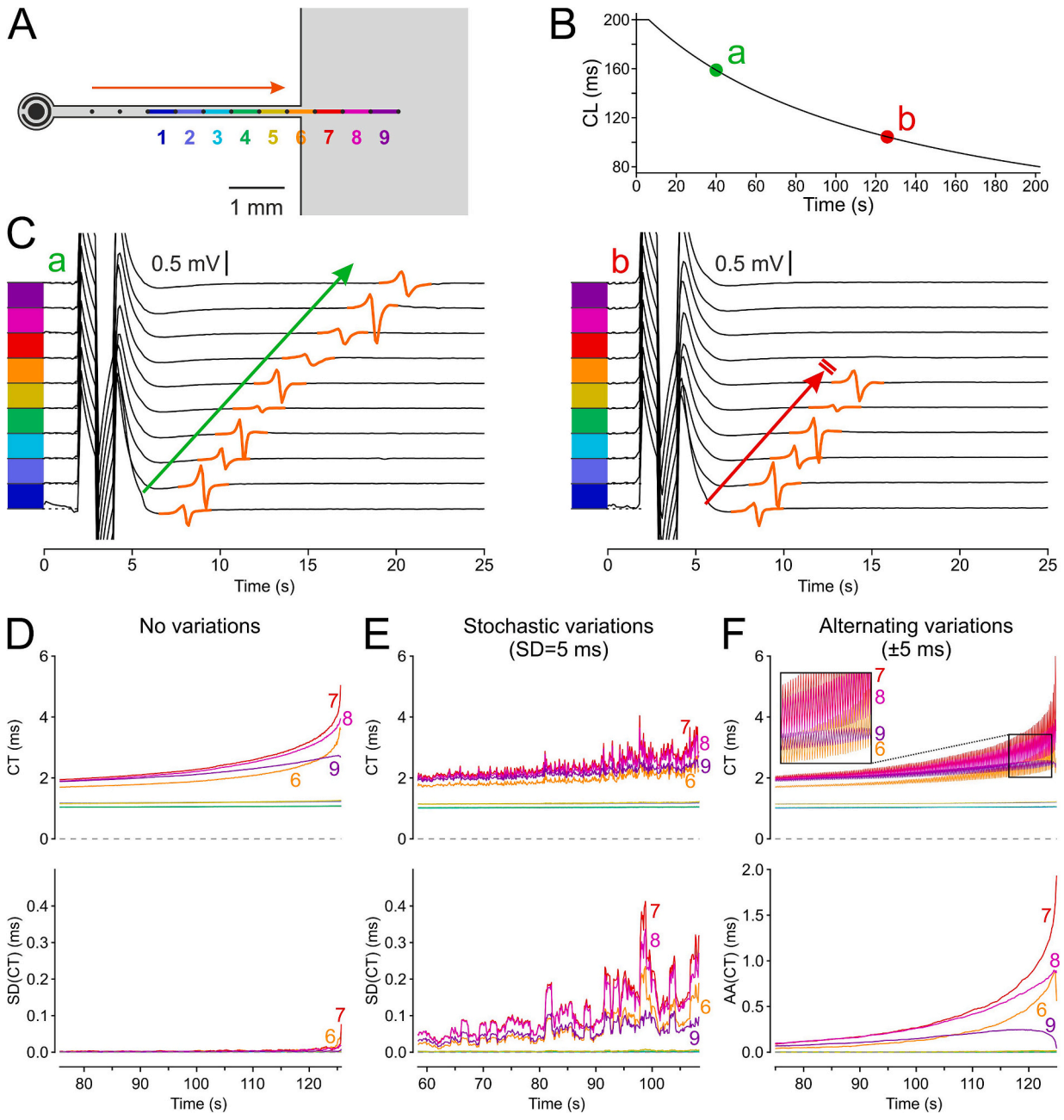

Fig. 3. Conduction variability across an expansion in a culture of neonatal mouse ventricular myocytes. A: Schematic of the preparation showing the recording sites and the corresponding intervals (1–9, color map) used to investigate CT. The stimulation dipole is depicted by the black structure on the left and the orange arrow denotes the direction of propagation. B: Ramp pacing protocol without variations. The green and red markers (a, b) correspond to the time points of the recordings presented in C, at the onset of the experiment and at the time of first block occurrence, respectively. C: Representative electrograms (highlighted in orange) showing a successfully propagated impulse (a, green arrow) and the first impulse that was blocked by the expansion (b, red arrow). Color-coding as in A. Stimulation artifacts are visible before the electrograms. D: Evolution of local CTs (top) and SD(CT) (bottom) during the pacing ramp without variations for the last 50 s before block occurred. E: Same as D, for the ramp with stochastic variations (SD of 5 ms). F: Evolution of local CTs (top) and AA(CT) (bottom) during the ramp with alternating variations (± 5 ms) for the last 50 s until block occurred. Color-coding and labeling as in A. Note the different ordinate axis for AA(CT) in F. (For interpretation of the references to color in this figure legend, the reader is referred to the web version of this article.)

CL of 104 ms. As expected from the current-to-load mismatch, local CTs were higher for the regions located at and after the expansion (intervals #6 to #9) indicating that the conduction was slower in these regions (Fig. 3D). For these specific intervals, the CTs also increased abruptly before the occurrence of conduction block (Supplemental Video S1). This increase was most prominent for intervals #6, #7 and #8 (at the expansion and the two following). However, in line with computer simulations, SD(CT) at the intervals #6 and #7 increased only for the last few impulses before block.

When the preparation was stimulated with the same ramp to which the stochastic CL variations were added (Fig. 3E, Supplemental Video S2), the first conduction block occurred at 108 s (earlier than during the control ramp), but at a similar CL of 103 ms. Consistently with simulation results, while the CTs themselves increased only mildly before conduction block, the SD(CT) exhibited a multiple-fold increase for intervals #6, #7 and #8 and #9, whereby the maximal increase occurred for intervals #6 to #8 (at and just after the expansion, respectively). Last, when the preparation was paced with the same ramp but with

alternating variations (Fig. 3F, Supplemental Video 3), the first conduction block occurred at the interval corresponding to expansion site after 125 s at a CL of 100 ms (similar to the control ramp). As in the simulations, alternating CL variations caused beat-to-beat alternations of CTs, as quantified by AA(CT), especially for intervals #6, #7 and #8. Again, these alternations became more and more prominent as the moment of the first block drew nearer, with a major increase for these latter intervals. Importantly, with both stochastic and alternating variations of CL, SD(CT) and AA(CT) for the intervals with unstable conduction exhibited a considerable increase already tens of seconds before the occurrence of conduction block, allowing for its relatively early anticipation.

3.3. *Stochastic and alternating pacing generate a gain in both anticipation performance and prediction precision*

To gain more insight about the behavior of conduction in our in vitro cardiac tissue expansions, we conducted a more in-depth analysis of these results. Specifically, SD(CT) and AA(CT) were considered as distributions over the interelectrode intervals, and we computed their first two moments (mean M_1 and standard deviation M_2) to estimate the site of block and evaluate the accuracy of this estimation. Our aim was to ascertain how many APs before the occurrence of block our approach could provide information regarding the instability of conduction. Because block did not occur at the same time or at the same CL in the different preparations (inter-preparation variability, see section 3.5 below), we therefore considered the count of stimuli before the first block. Fig. 4 shows this analysis for the different pacing protocols in the form of heat maps for the last 400 APs before block occurred (same experiment as in Fig. 3). For every pacing stimulus, the distribution of SD(CT) or AA(CT) was normalized such that their sum over all intervals equals 1 (of note, this normalization does not affect M_1 and M_2 but permits a better visualization). M_1 as well as $M_1 + M_2$ and $M_1 - M_2$ (corresponding to mean ± SD) are plotted on top of the heat maps.

In accordance with the observations reported in Fig. 3, normalized sliding SD(CT) performed poorly in identifying the region of unstable conduction near the expansion when no variations were applied to the pacing ramp (Fig. 4A). In contrast, introducing stochastic variations with a SD of 2 ms allowed to better localize the region of unstable conduction, as illustrated by the sharper contrast discriminating between regions with low SD(CT) (in dark blue) and high SD(CT) (in yellow), and as reflected by the more stable M_1 and the relatively lower M_2 (Fig. 4B). Noteworthy, this discrimination is already visible 400 beats before the block occurrence, allowing for its anticipation. Increasing the amplitude of stochastic CL variations to a SD of 5 ms allowed the region of unstable conduction to appear even more evidently (Fig. 4C). On the one hand, estimations of M_1 using the pacing ramp without variations tended to erroneously appear near the center of the row of electrodes and with a high M_2, because the distribution of SD (CT) (which was low) was widely spread over all intervals, only evolving towards the region near the expansion shortly (~100 impulses) before block occurred. On the other hand, with stochastic variations, M_1 pointed out the interval colored in red, right after the interval of effective block, with a low M_2 already 400 APs before block, indicating that the estimation gained in precision.

Similar results were obtained when comparing the control ramp and the ramps with alternating variations while using AA(CT) as a marker. While the performance of M_1 using AA(CT) was poor and erratic without

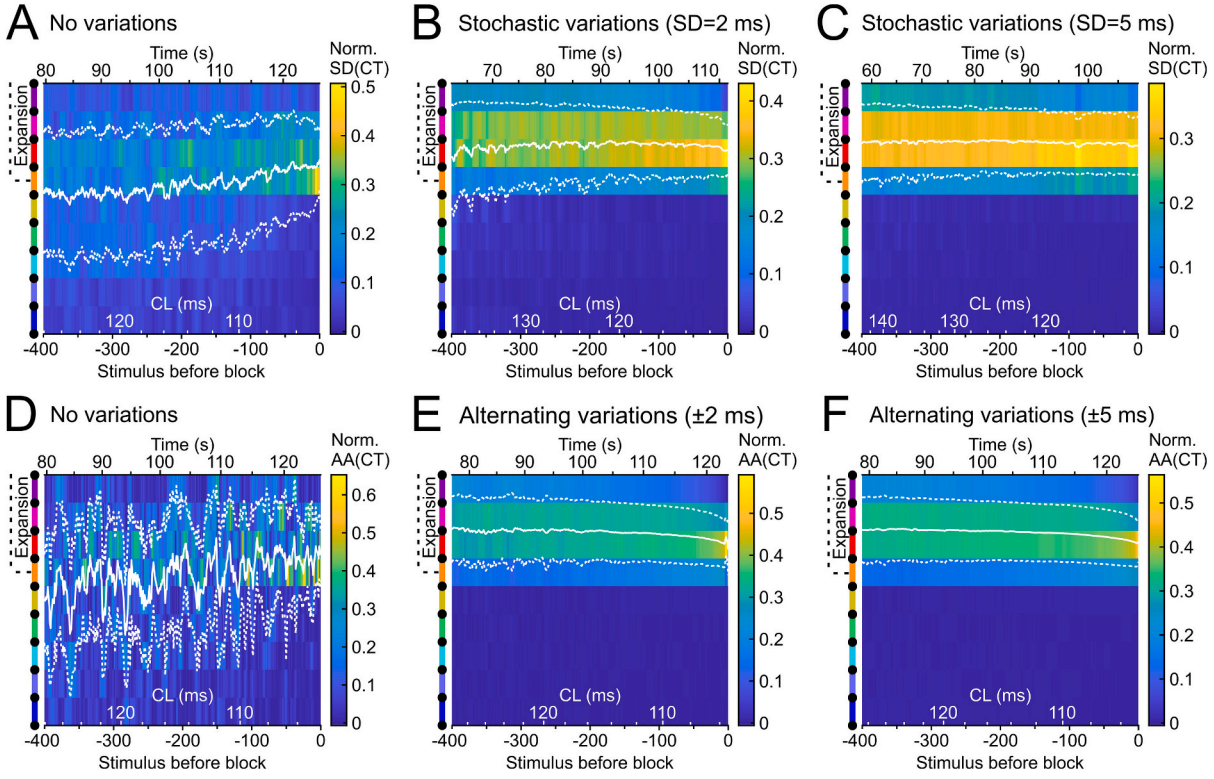

Fig. 4. SD(CT) and AA(CT) performance as predictive markers of conduction block. A, B and C: Analysis for the pacing ramp without variations, with stochastic variations with a SD of 2 ms and with stochastic variations with a SD of 5 ms, respectively. The heat maps show the evolution of the normalized sliding SD(CT) for each recording interval (color-coded on the left as in Fig. 3), over the course of the last 400 stimuli before the first conduction block occurred. Time within the pacing ramp is represented by the axis above each individual panel, and CL is represented on the bottom with white tickmarks and fonts, respectively. The expansion region is represented by the dotted line on the top left. The white solid lines represent the first moment M_1 (mean of the distribution of SD(CT) values over the interelectrode intervals) as an estimator of the site of block. The dotted white lines represent the second moment M_2 (standard deviation of the distribution around M_1) providing a measure of the accuracy of the estimation. D, E and F: Same as A, B and C, but using AA(CT) for the ramp without variations, the ramp with alternating ± 2 ms variations and the ramp with alternating ± 5 ms variations, respectively.

pacing variations (Fig. 4D), introducing pacing alternations of 2 ms and 5 ms induced a stable M_1 with a low M_2 already 400 stimuli before block (Fig. 4E and F). Interestingly, in this preparation, with both the stochastic and alternating versions of the pacing protocol, the region with the largest SD(CT) and AA(CT) as identified by M_1 was not at the interval bridging the expansion but just after it. This observation is similar to that in the simulations (Fig. 2).

Figure 5 shows a superimposition of the first and second moment traces to better illustrate these findings. Introducing stochastic or alternating pacing variations led to a stable estimate of M_1 (Fig. 5A and B, respectively) with a smaller M_2 (Fig. 5C and D) already hundreds of impulses before block. In both stochastic and alternating pacing conditions, increasing the amplitude of the variations did not yield different estimations regarding the site of block (almost overlapping traces). There was a minor improvement in M_2 with the stochastic protocols when the SD of pacing CL variations was increased from 2 to 5 ms, but no manifest difference for the protocols with alternating variations when the latter were increased from $\pm$ 2 to $\pm$ 5 ms. Furthermore, both types of protocols yielded similar results in terms of M_2.

3.4. Stochastic and alternating pacing approaches to assess cardiac conduction stability are reproducible in tissue expansions

To assess the reproducibility of these results, the same investigations were conducted with 7 different preparations. The heat maps in Fig. 6 show the evolution of M_2 for the stochastic and alternating ramp pacing protocols over the final 400 beats preceding block. In this analysis, the M_2 values obtained with the protocols with variations were normalized against the M_2 values obtained with the control ramp. Thus, values <1 indicate that M_2 was lower with the corresponding protocol with variations and reflect a better performance. For every preparation tested, M_2 values were lower when stochastic variations with a SD of 2 ms were added to the pacing ramp (Fig. 6A), except for one preparation (preparation 2) in the range 400 to 220 stimuli before block. This result indicates a finer estimation of the conduction block site. This became more pronounced with stochastic variations having a SD of 5 ms, as characterized by the darker blue appearance of the heat map. Moreover, the stochastic pacing approach also performed well for preparation 2. Of note, for the first 3 preparations, heat maps exhibited a deeper blue shade as conduction block drew nearer, indicating a faster enhancement in precision with the addition of stochastic variations to the pacing ramps. Similarly, estimations of the site of conduction block were also more precise when alternating variations were implemented (Fig. 6B). Increasing the amplitude of these alternating variations from 2 ms to 5 ms had only a minimal impact on the heat map appearance, aligning with observations from Fig. 5D. Of note, for low amplitude variations (2 ms), alternating pacing performed better (lower normalized M_2) to anticipate the site of conduction block, as compared to stochastic pacing.

Coherently with the relatively higher M_2 values, M_1 values obtained with pacing ramps without variations were disparate, fluctuating over a wide range irrespectively of whether SD(CT) or AA(CT) was used to compute it (Fig. 6C and D, respectively). On the contrary, M_1 derived from pacing ramps with stochastic variations of CL were more stable and homogeneous (Fig. 6C). The evolution of M_1 during pacing with alternating variations also exhibited stability and homogeneity (Fig. 6D). Interestingly, M_1 values derived from both stochastic and alternating pacing ramps tended to converge to a position situated 0.5–1

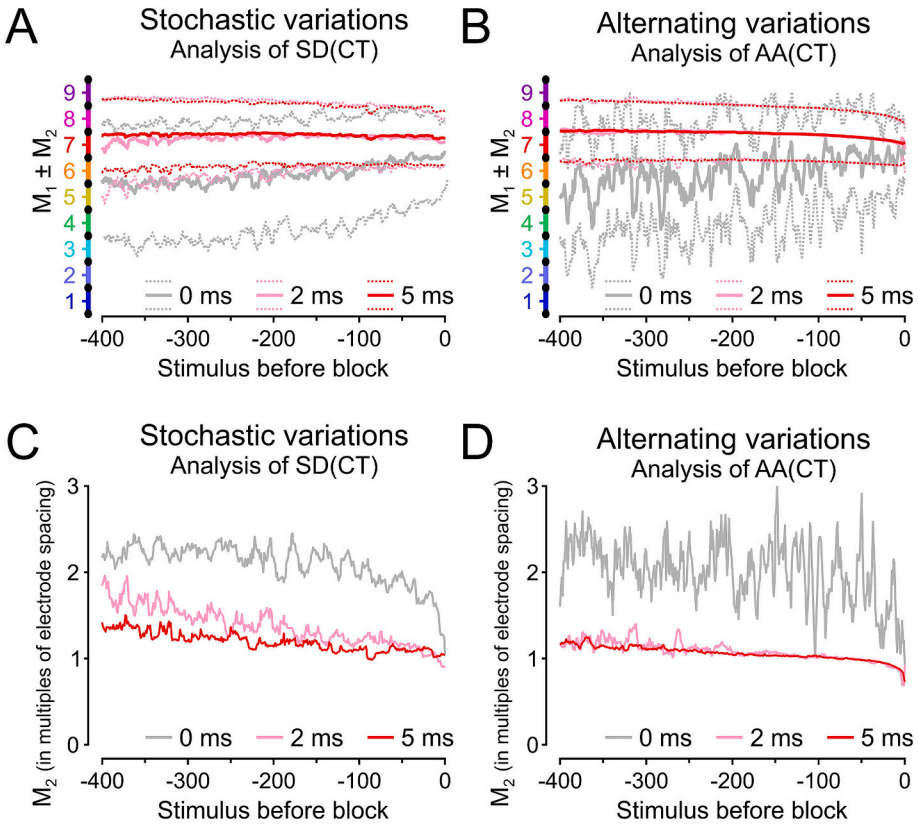

Fig. 5. Prediction of conduction block location in vitro. A: Evolution of the first moment M_1 (bold traces) and their corresponding second moment intervals $M_1 + M_2$ and $M_1 - M_2$ (thin traces) computed based on SD(CT) for ramp pacing protocols without variations (grey), and with stochastic variations with a SD of 2 ms (pink) and 5 ms (red) for the last 400 stimuli before conduction block. B: Same as A, with M_1 and M_2 computed based on AA(CT) for ramp pacing protocols without variations (grey), and with alternating variations of 2 ms (pink) and 5 ms (red). C: Evolution of M_2 (as a multiple of electrode spacing), computed based on SD(CT) for the data in A. D: Same as C, for M_2 computed based on AA(CT) for the data in B. (For interpretation of the references to color in this figure legend, the reader is referred to the web version of this article.)

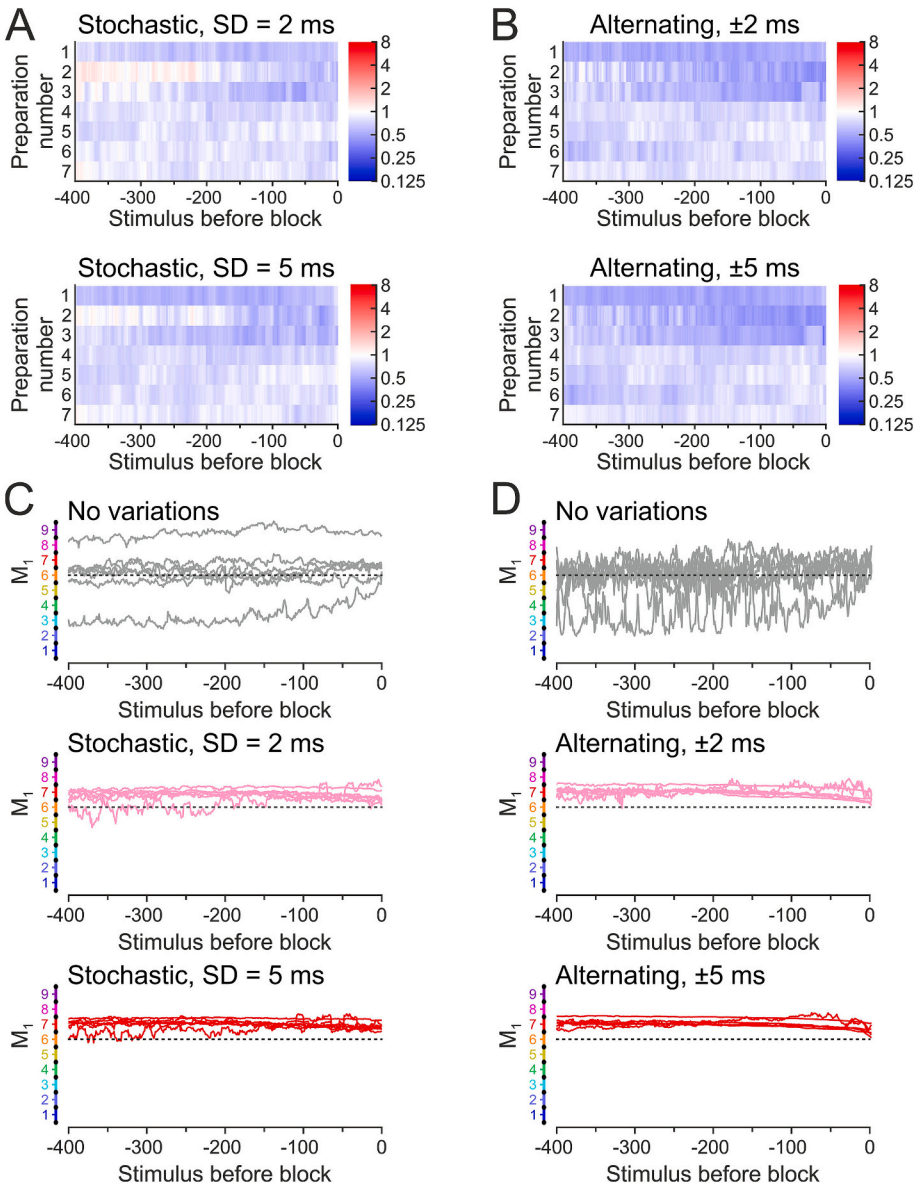

Fig. 6. Meta-analysis of predictive markers performance in all preparations during stochastic and alternating pacing. A: Heat maps showing for every preparation ($n = 7$, from 6 distinct cultures) the evolution of M_2 over the last 400 beats before conduction block during ramp pacing protocols with stochastic variations with a SD of 2 ms (top) and with a SD of 5 ms (bottom). M_2 obtained with the protocol with variations was normalized to M_2 obtained with the control protocols without variations. Note the logarithmic color scale, with blue hues corresponding to <1 and red hues to >1. M_2 was computed using SD(CT). B: Same as A, for ramp pacing protocols with alternating variations of ± 2 ms (top) and ± 5 ms (bottom). M_2 was computed with AA(CT). C: Evolution of M_1 in all individual preparations over the 400 beats before conduction block during ramp pacing protocols without variations (grey, top) and with stochastic variations with a SD of 2 ms (pink, middle) and 5 ms (red, bottom). M_1 was computed using SD(CT). The dotted line indicates the actual site of the expansion. D: Same as C, during ramp pacing protocols without variations (grey, top) and with alternating ± 2 ms variations (pink, middle) and ± 5 ms variations (red, bottom). M_1 was computed using AA(CT). (For interpretation of the references to color in this figure legend, the reader is referred to the web version of this article.)

interelectrode interval (0.25–0.5 mm) beyond the actual site of the expansion (dotted line), which was, for all preparations, in the center of interval #6. The location identified by M_1 thus corresponds to the first electrode within the expanding region or to the beginning of the following interelectrode interval. These results are in line with the observations made in Figs. 4 and 5. Importantly, in a majority of experiments with alternating variations, M_1 approached the center of interval #6 during the last 100 stimuli before block, suggesting that AA(CT) performs more accurately as a predictive localization marker when block is imminent.

Altogether and consistently with in silico investigations, this series of experiments supports the notion that predictive markers for the localization and the occurrence of conduction block can be derived experimentally using pacing with stochastic or alternating variations. This conduction block can be anticipated by monitoring SD(CT) and AA (CT).

3.5. *The role of restitution during stochastic and alternating pacing*

The restitution of conduction velocity (CV) and AP duration (APD) are important factors in arrhythmogenesis. Steep CV and APD restitution slopes can undermine the stability of conduction and promote alternans, wavebreaks, and thus reentrant arrhythmias [33]. Therefore, to gain deeper insight into the mechanisms causing increased SD(CT) and AA (CT) during stochastic and alternating pacing, we examined in more detail the restitution properties of CV, CTs and, in the simulations, of

APD.

Figure 7A shows CV (determined in the proximal part of the strand) vs. instantaneous CL for all pacing protocols (until block occurred) and for all individual experiments. Of note, because of biological inter-preparation variability, the individual preparations exhibited different CVs both at the onset of the pacing protocols (plateau) and at the first occurrence of block. However, all individual restitution plots exhibited a similar pattern, with an overall positive slope, a relatively shallow slope at larger CLs, and a steeper slope at shorter CLs as the conduction block drew nearer. Baseline plateau CVs ranged from 29 to 50 cm/s, minimum CVs from 27 to 45 cm/s and the CLs at which the first block occurred ranged from 80 to 165 ms. The CV values at longer CLs are consistent with those reported for similar wild-type preparations in former studies by both our group [20,23,34] and other investigators [35,36].

Figure 7B depicts CV and APD in the computer model (for this analysis, an unbranched 100-element long and 5-element wide strand (6 mm long, 300 μm wide) was simulated and these parameters were measured in its center). This Figure shows that the model exhibited a CV restitution behavior representative of the cultured preparations. Importantly, introducing beat-to-beat variations of the pacing CL did not affect the general behavior of CV restitution, neither in the simulations, nor in the experiments, except for slightly more disparate or alternating values during ramps with stochastic and alternating variations, respectively. In the model, APD restitution was present but weak, with a slope around 0.17, which is too low to induce alternans [33].

To explain the generation of large SD(CT) and AA(CT) at sites vulnerable to block, it is insightful to represent CTs at the individual spatial intervals vs. CL, as shown for the pacing protocols without variations in Supplemental Fig. S3. This Figure not only shows that CT (which is inversely proportional to local CV) was globally larger for the intervals at and just after the expansion, but it also shows that for these sites, CT typically increased earlier as CL was decreased. This increase was caused by the enhancement of CV restitution due to the current to-load mismatch. Thus, at such sites, both CV and CV restitution are modulated by the current-to-load mismatch. The resulting CT restitution curves exhibit a negative slope, which is steepest at short CLs. Hence, this negative slope accounts for the large SD(CT) and AA(CT) observed at the site of current-to-load mismatch.

4. Discussion

We propose a new paradigm to evaluate the stability of conduction at sites of current source-to-load mismatch and thus to identify sites where conduction is prone to block. To test this paradigm, non-conventional pacing protocols consisting of pacing ramps incorporating stochastic or alternating CL perturbations were applied to challenge conduction in both simulated and cultured expansions of cardiac tissue. As hypothesized, when such perturbations were introduced, the decrease in stability preceding conduction block led to significant and progressively increasing variations of local CTs at sites where source-to-load mismatch and depolarization reserve were critical. This response to perturbations thereby permitted to identify the site where conduction was the most prone to block. We identified SD(CT) (during stochastic pacing) and AA (CT) (during alternating pacing) as markers of conduction instability. Subsequently, from these two metrics, we derived M_1 and M_2, which respectively provided an estimation of the site of conduction block and the accuracy of this estimation. Importantly, in contrast to control ramps, stochastic and alternating variations induced an early increase of SD(CT) and AA(CT) allowing for the anticipation of conduction block. Pacing variations also resulted in more stable M_1 estimations and in an increased accuracy (decreased M_2 values).

The present work constitutes a proof-of-principle study to validate our approach. As cardiac expansions represent typical structures known to exhibit current source-to-load mismatch and conduction block [2,18–20], these geometrical structures served as appropriate benchmarks to test our hypothesis regarding conduction behavior during stochastic and alternating pacing.

4.1. Comparison to previous studies

In a computer modeling study, Aslanidi et al. [13] examined the safety factor (SF) of propagation in two- and three-dimensional models of the expansion of a Purkinje fiber into the myocardium, a site that is classically considered prone to arrhythmogenic unidirectional block [37]. They observed a local increase of the SF around and just after the expansion site, and they interpreted this paradoxical increase to an accumulation of charge due to the current source-to-load mismatch [13]. They also observed a biphasic relationship between CV and the SF near the expansion [13]. However, the authors used the earlier SF formulation of Romero et al. [15,16], which is based on the definition by Shaw and Rudy [9] and which was initially developed for 1-dimensional tissue. Therefore, the SF computation by Aslanidi et al. [13] did not consider the direction of propagation relative to the discrete grid used for simulations, as proposed later by Romero et al. [10]. Hence, the local increase of the SF around and just after the expansion site could possibly be an artifact. In an exploratory simulation, we computed the SF across the expansion after 30 cycles of pacing at a CL of 200 ms without CL variations using the latter formulation by Romero et al. [10]. As shown in Supplemental Fig. S4, the SF was decreased about 1 mm before and after the expansion site, with a minimum in the first column of excitable elements inside the expansion.

In the past, the counterintuitive behavior of the SF motivated Boyle and Vigmond [11] to elaborate a new definition of the SF, which considers explicitly the excess charge delivered to a cell relative to the minimum required to induce an AP. This new formulation resolved the apparent paradoxical behavior reported by Aslanidi et al. [13]. Interestingly, the data of Boyle and Vigmond [11] show that during successful propagation across a rectangular tissue expansion, the region with the lowest SF is not located at the expansion site, but a fraction of a millimeter further inside the expansion. This observation also applies to the results of a further study by the same research team [12]. In our present study, we typically observed the largest SD(CT) and AA(CT) not for the interelectrode segment bridging the expansion, but for the subsequent segment in both simulations and experiments (see Figs. 2 and 3, respectively). Moreover, our analysis of experimental data using the first moment M_1 showed that this moment points to a site about 0.5 mm beyond the actual geometrical expansion (see Fig. 6). Thus, our analysis of conduction stability is more consistent with the SF analysis of Boyle and Vigmond [11,12] than with the formulation of Romero et al. [10].

The reason why the site with the lowest SF or the highest conduction instability is not exactly located at the geometrical expansion may be related to the combination of two factors causing source-to-load mismatch: the expansion itself and the curvature of the depolarization wavefront once it has passed the expansion. Indeed, by causing divergence of the local circuit current, convex wavefronts lead to slow conduction and even block [38]. In previous simulations of conduction across an expansion, Fast et al. have shown that the region of slowest conduction (with crowding of isochrones) can be located about 0.25 mm after the expansion [39]. Thus, our results align with the findings of these previous studies.

Using simulations of conduction in whole rabbit ventricles, Boyle et al. [40] demonstrated that premature ectopic stimulation together with a reduction of the sodium current (I_{Na}) exacerbates arrhythmogenic slow conduction and block at low SF sites associated with an abrupt increase of myocardial wall thickness. In the present study, we used a progressive decrease of pacing CL to depress I_{Na} availability to unmask sites of unstable conduction. Hence, our results are also in line with these earlier findings.

4.2. Effect of propagation direction

As highlighted by the simulations of retrograde conduction (from the

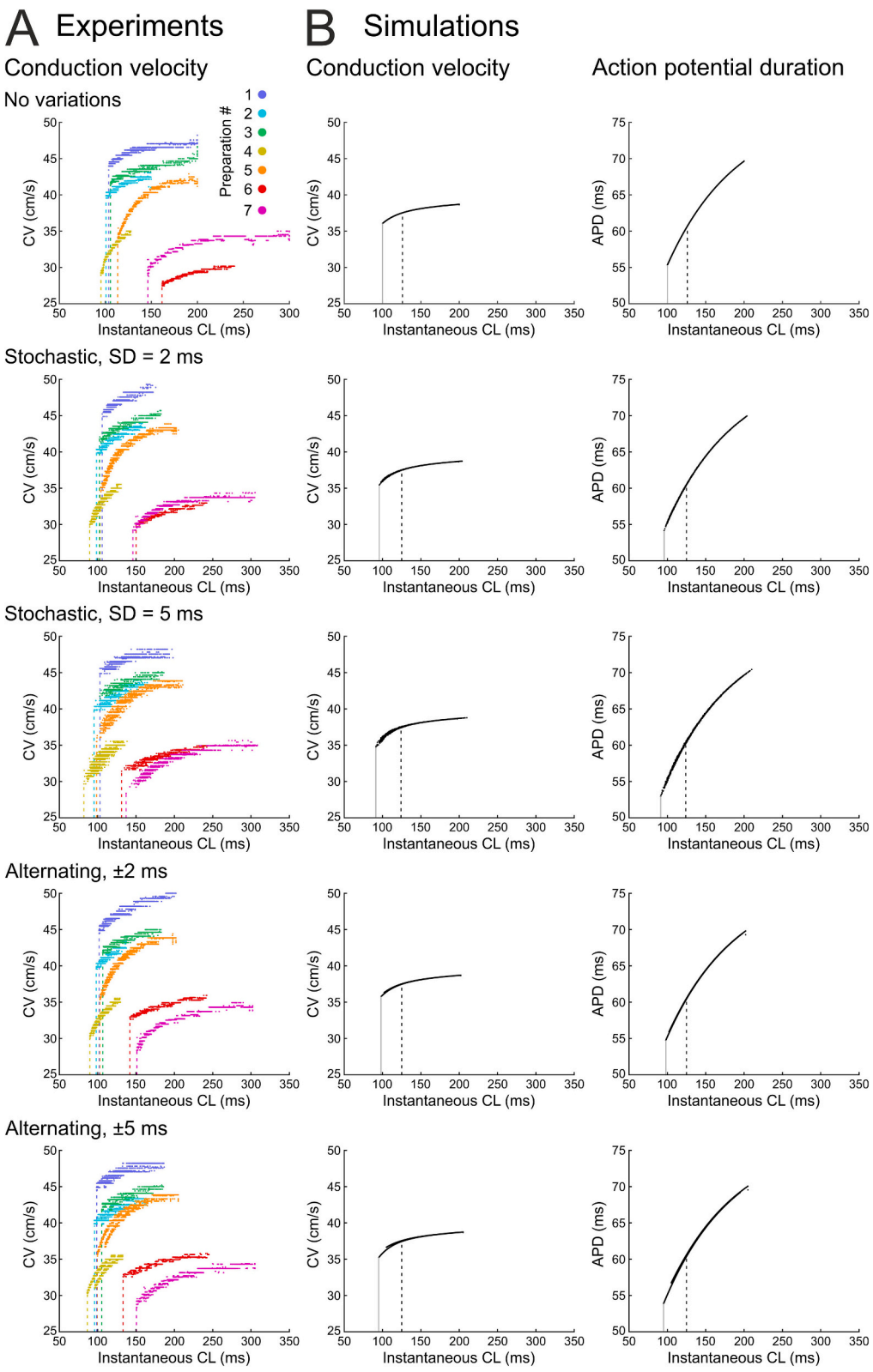

Fig. 7. Restitution of conduction velocity (CV) in experiments, and of CV and AP duration (APD) in simulations. A: CV vs. instantaneous CL for every ramp pacing protocol used in this study (from top to bottom: ramp without variations, ramp with stochastic variations with a SD of 2 ms and 5 ms, and ramp with alternating variations of ± 2 ms and ± 5 ms). Data for every individual preparation are plotted in a different color (legend in the top panel). Preparation 1 was used for the analyses shown in Figs. 3, 4 and 5. The vertical dotted lines indicate the CL at which the first conduction block occurred. B: CV and APD vs. instantaneous CL for simulations of conduction for the same ramp pacing protocols as those used in Fig. 2. For these simulations, a non-expanding 6-mm long strand was used and CV and APD were measured in the center. The vertical grey lines indicate the minimum CL at which conduction was sustained in the non-expanding strand, and the dotted lines indicate the CL at which the first block occurred in the expanding strand (see Fig. 2).

expansion to the strand), conduction blocks at tissue expansions were unidirectional, in agreement with previous reports at high stimulation rates at geometrical expansions of cultured rat neonatal ventricular tissue [19,32]. Retrograde propagation was still successful at CLs at which propagation failed in the antegrade direction. Moreover, for stochastic and alternating ramp pacing protocols, no increased variability of local CTs was detected near the expansion-strand junction during retrograde propagation. At higher pacing rates, the stimuli eventually failed to generate propagating APs. In a subsequent study, it was shown that decreasing depolarization reserve with tetrodotoxin or nifedipine induced conduction delays and unidirectional blocks specifically at the expansion during antegrade propagation, but had only a negligible effect on retrograde propagation [41]. As opposed to convex antegrade activation wavefronts past the expansion, retrograde wavefronts were shown to be planar, with conduction accelerating in the narrow cell strand. Moreover, retrograde conduction was characterized by monophasic and evenly spaced AP upstrokes. Our simulations are in line with these observations.

As unidirectional blocks are causal factors in reentrant arrhythmogenesis [2], it is important to note that our approach could allow for a relative comparison of propagation in both antegrade and retrograde directions. Computing the variability of conduction in both directions might then be insightful to determine if there is a propensity for unidirectional block.

4.3. How accurately can block be located?

First, in both simulations and experiments, it must be pointed out that the exact location of unstable conduction depends on how activation time and conduction time are exactly defined. Depending on the definition used for activation time (e.g., maximum upstroke velocity, peak I_{Na}, time at 50 % of AP amplitude, minimum of the derivative of the extracellular potential), sensibly different values of activation time can be obtained, especially at an expansion [19]. For our experiments, we directly computed CT using the algorithm of Shors et al. [31], which bypasses the determination of activation times. All these factors may impact on the analysis of SD(CT) and AA(CT). Second, the exact site of block also depends on how block is defined. Across an expansion of tissue that is well coupled with gap junctions, the blocked AP evolves into responses of progressively decreasing amplitude (see Fig. 2), making the exact identification of the site of block arbitrary because it will depend on its definition. This region of decaying amplitude can span a region in the range of the space constant, which, in cardiomyocyte cultures, has been estimated to be 360 μm [42]. This value represents a plausible estimation of the best accuracy with which block location can be determined.

In our experiments, the interelectrode spacing was 500 μm, which is in the range of the space constant. For impulses that were blocked by the current-to-load mismatch, we observed that the last electrogram that could be detected occurred in all experiments at the electrode located immediately before (0.25 mm) the expansion site (see Fig. 3C). The absence of any detectable electrogram at the next electrode, located 0.25 mm after the expansion, suggests that the block was located somewhere in the interval spanning these two electrodes (interval #6 in Fig. 3). This seems to be at odds with the notion that the site of most unstable conduction is located just after the expansion. One possible explanation to resolve this discrepancy is that block indeed occurred just after the expansion, but the extracellular signal became undetectable because the I_{Na} of the decaying electrotonic response was then only very weak.

Based on these considerations, a precision in the range of 0.5 mm (corresponding to the interelectrode interval and coherent with the second moment M_2) appears reasonable. This precision would certainly be sufficient in a clinical setting, as electrode spacing in mapping catheters and the size of ablation lesions are usually larger than 1 mm [43,44].

4.4. Design of the pacing ramps

Our pacing ramps were designed to produce a steeper decrease of CL at the onset of the pacing ramp, followed by a more and more progressive decrease with time (Fig. 1B). In further applications, possibly with preparations from other species, it may be important to have some a priori knowledge of the range of CL at which conduction block occurs, in order to make this range lie within the flatter part of the pacing ramp and hence to avoid approaching the moment of block too quickly. Adjusting the pacing ramp accordingly will thus allow for an earlier anticipation of the moment and site of conduction block.

In terms of relating effect size (the magnitude of SD(CT) and AA(CT)) to CL variability (2 or 5 ms in our study), it is worth to consider the slope of the CT vs CL relationship (Supplemental Fig. S3). Based on our previous work [34,45], we can expect SD(CT) and AA(CT) to be proportional to both the amplitude of CL variations and to the slope of the CT restitution function. However, with repeated variations of CL, this proportionality is further modulated by APD restitution [34,45]. Because each preparation is different due to biological variability, these slopes and the effect size cannot be anticipated a priori. For the choice of the magnitude of pacing CL variations, sufficiently large values must be chosen to yield detectable SD(CT) and AA(CT). However, excessive pacing CL variations may induce very short CLs that could potentiate block already at the onset of the protocol. The choice of the magnitude of CL variations must therefore be decided empirically, and we found that values of 2 and 5 ms (a few percent of the CL at which block occurs) were well suited in our setting.

4.5. Future developments and clinical perspectives

By relying on the simple pragmatic notion that sites of unstable conduction are sensitive to perturbations, our approach has the strength of being straightforward to implement in any setting from in vitro to ex vivo and in vivo studies. The analyses that we present here are computationally undemanding and could be easily executed in real-time applications. Our approach also bypasses the laborious evaluation and computation of the SF, which is in principle feasible in vitro (albeit with a number of assumptions) [12] but would hardly be feasible in vivo. Moreover, our approach minimizes the risk of causing block during detection of unstable conduction, which would be beneficial in potential clinical applications. With a classical S1-S2 protocol, the coupling S1-S2 interval would probably need to be shortened more substantially than a few milliseconds to provide useful information in terms of susceptibility to block, hence augmenting the risk of actually inducing the block and precipitating reentry.

In our proof-of-concept study, we investigated conduction across tissue expansions as classical geometrical structures causing source-to-load mismatch. Future work will need to evaluate whether our approach can also identify unstable sites in settings in which block cannot be anticipated a priori, such as in the presence of heterogeneous fibrosis, ischemic regions or heterogeneous expression of channels. In vitro, this could be tested, e.g., in co-cultures of cardiomyocytes and myofibroblasts, or in co-cultures of wild-type and connexin 43 knockout ventricular myocytes, which are highly prone to heterogeneous conduction and block [23]. In the future, our approach should also be validated using different shapes of expansions, e.g., with a more progressive transition between the strand and the bulk tissue. Noteworthy, identifying sites of potential block is a relevant clinical need for the management of patients presenting with atrial and ventricular tachyarrhythmias. In a clinical setting, our pacing paradigms may already provide valuable information by using one stimulation catheter and a second one with a linear arrangement of electrodes. Techniques based on more complex catheters with a two- or three-dimensional arrangement of electrodes undeniably represent an additional challenge regarding the analysis and interpretation of the results, but this aspect opens perspectives for future basic studies using e.g., heterogeneous

tissue cultured in vitro and mapping with a two-dimensional array of electrodes.

In previous work, we showed that pacing at stochastic or alternating CLs can provide information regarding the restitution properties of CV and APD, and thus of electrical alternans, a known arrhythmogenic mechanism [26,34,45]. In that work, we observed that the largest effects are observed for pacing at alternating intervals and suggested that this approach may facilitate the identification of conduction heterogeneities [34,45]. In agreement with our previous findings, our expansions were very sensitive to alternating perturbations allowing for earlier anticipation of block. Moreover, by its deterministic nature, pacing with alternating CL performed better than stochastic pacing to yield a regularly increasing AA(CT) for the regions of unstable conduction (see Fig. 3), even with pacing CL variations as small as ± 2 ms (see Fig. 6). By being simpler and deterministic, pacing protocols with alternating CLs may also find more acceptance in the clinical community.

In that same work [34,45], we reported that a positive CV restitution slope leads to an attenuation of interbeat interval (IBI) variability in the presence of stochastic or alternating pacing CL variations (IBIs being defined at a specific location as the series of differences between activation times). The question therefore arises whether it would be in principle possible to identify two successive sites of vulnerable conduction with our approach. To answer this question, we plotted in Supplemental Fig. S5 the standard deviation of the last 10 interbeat intervals (IBIs) before block occurred (SD(IBI)) vs. position along the axis of the preparations during stochastic ramps, as well as the amplitude of alternating IBI variations (last 10 IBIs before block, AA(IBI)) vs. position during alternating pacing ramps. Consistent with our previous work, this analysis revealed an attenuation of both SD(IBI) and AA(IBI) with increasing distance from the pacing site, with a marked decrease across the expansion. Of note, although SD(IBI) and the AA(IBI) became smaller after the expansion, they remained in most cases still sufficient to permit, in principle, the detection of another site of vulnerable conduction further downstream, especially for pacing protocols with stochastic SD = 5 ms or alternating ± 5 ms CL variations.

4.6. Limitations

One limitation of our approach is that a direct comparison between the various formulations of the SF [9–12] and the metrics that we developed in our study is not possible experimentally. Hence, a one-to-one mapping function between them cannot be established. Such a mapping function would also depend on the exact situation causing unsafe or unstable conduction (e.g., geometrical factors, regions with decreased excitability, fibrosis, etc). Our metrics are relative rather than absolute in the sense that there is not a determined threshold for SD(CT) or AA(CT) at which block occurs. Nevertheless, they permit to locate the site of most unstable conduction via relative comparisons with regions of stable conduction.

One other potential limitation of our approach, which will need to be evaluated in future studies, concerns its practical clinical implementation. This implementation may face a number of challenges given the more complicated 3-dimensional architecture of endocardial surfaces and the limited resolution of exploratory catheters. On the one hand, the clinical determination of CV and of CTs relies on an accurate measurement of activation times and a precise registration of the mapping points. Recently, it was shown that 2-dimensional CV mapping of the myocardial surface leads to overestimation of the 3-dimensional CV if the analysis assumes that impulses propagate along a single layer and orientation, thus neglecting the participation of in-depth propagation, and because 2-dimensional CV vectors are unlikely to be oriented parallel to the endocardial surface [46]. On the other hand, our approach relies on relative comparisons of CTs and we surmise that normalized markers (such as the ratio of SD(CT) over mean CT (coefficient of variation) or the ratio of AA(CT) over mean CT) may function equally well, which has the potential to circumvent the issue of precise CT determination. Regarding the limited resolution of exploratory catheters, we do not expect that our approach will lead to a higher spatial resolution in localizing unstable conduction sites than that given by interelectrode distance (see "4.3. How accurately can block be located?"). Nevertheless, a resolution of a few mm may already be useful in identifying arrhythmogenic substrates. We do not know to which extent our 2-dimensional simulations and experiments can be extrapolated to the 3-dimensional geometry in intact myocardium, but based on the biophysics of AP propagation across a current-to-load mismatch, we expect our findings to be applicable in this setting, at least qualitatively. Finally, the analysis of IBIs presented in Supplemental Fig. S5 suggests that it may be possible to locate consecutive sites of unstable conduction, a scenario that is possible in the diseased myocardium in vivo. In our study, we leveraged the possibility to conduct long-term experiments by using microelectrode arrays. A state-of-the art technique in cardiac electrophysiology is optical mapping of membrane potential using fluorescent reporters [47,48]. However, a problem with optical mapping is the photodynamic damage that can arise during extended (minutes) and repeated illuminations and the resulting run-down of the preparation with progressively altered conduction, which would render the results difficult to interpret. Optical mapping would then also make comparisons between different protocols in a given preparation impossible. Moreover, optical signals recorded with such techniques are prone to noise, which may alter the precision of the determination of activation and conduction times. Our approach may therefore be challenging to implement in this context.

Finally, for our simulations, we used a modified version of the Luo-Rudy I model [22] rather than a more elaborate (but more computationally expensive) electrophysiological model. However, the key biophysical properties that underlie our pacing approaches are the behavior of conduction in the presence of a structural source-to-load mismatch, and the existence of a relative refractory period during which depolarization reserve is restricted. Because all recent models possess these properties, we surmise that results will be qualitatively similar with such models, and a fortiori with other types of cardiac preparations.

5. Conclusion

We have developed and explored, for the first time to our knowledge, an innovative approach based on pacing at stochastic or alternating intervals to examine the stability of conduction and to anticipate the site where conduction is most prone to block. Our paradigm resides on the simple and pragmatic notion that sites with the most unstable conduction are those that are the most sensitive to repeated beat-to-beat perturbations in the pacing protocol. Reentry and fibrillation typically result from functional block in pathologically heterogeneous myocardium, and, therefore, there exists a clinical need to better identify such sites. Hence, the strategies presented here may open new avenues for basic and translational applications.

Supplementary data to this article can be found online at https://doi.org/10.1016/j.yjmcc.2024.10.007.

Funding

This study was supported by the Swiss National Science Foundation (grants 310030-184707 and 320030-227774 to J.P.K.).

CRediT authorship contribution statement

Stephan De Waard: Writing – review & editing, Writing – original draft, Visualization, Validation, Methodology, Investigation, Formal analysis, Data curation. **Helene Hinnen:** Writing – review & editing, Resources, Project administration, Methodology. **Jan P. Kucera:** Writing – review & editing, Writing – original draft, Visualization, Validation, Supervision, Software, Resources, Project administration, Methodology, Investigation, Funding acquisition, Formal analysis, Data

curation, Conceptualization.

Declaration of generative AI and AI-assisted technologies in the writing process

The authors did not use generative AI or AI-assisted technologies in the preparation of this work (except checking grammar and spelling).

Declaration of competing interest

None.

Data availability

The raw data, the MATLAB code for data analysis and simulations and the MATLAB scripts used to generate the figures are available on the repository Zenodo (https://dx.doi.org/10.5281/zenodo.13959653).

Acknowledgements

We are grateful to Michael Känzig and Elia Hänni for taking care of our animals, and to Christian Dellenbach and Hans Ruchti for trouble-shooting electronic and IT equipment.

References

[1] D.M. Bers, Cardiac excitation-contraction coupling, Nature 415 (2002) 198–205.
[2] A.G. Kléber, Y. Rudy, Basic mechanisms of cardiac impulse propagation and associated arrhythmias, Physiol. Rev. 84 (2004) 431–488.
[3] G.Y. Lip, L. Fauchier, S.B. Freedman, I. Van Gelder, A. Natale, C. Gianni, et al., Atrial fibrillation, Nat. Rev. Dis. Primers 2 (2016) 16016.
[4] R.S. Wijesurendra, B. Casadei, Mechanisms of atrial fibrillation, Heart 105 (2019) 1860–1867.
[5] B. Surawicz, Ventricular fibrillation, J. Am. Coll. Cardiol. 5 (1985) 43B–54B.
[6] J.P. Empana, I. Lerner, E. Valentin, F. Folke, B. Bottiger, G. Gislason, et al., Incidence of sudden cardiac death in the European Union, J. Am. Coll. Cardiol. 79 (2022) 1818–1827.
[7] C. Delgado, B. Steinhaus, M. Delmar, D.R. Chialvo, J. Jalife, Directional differences in excitability and margin of safety for propagation in sheep ventricular epicardial muscle, Circ. Res. 67 (1990) 97–110.
[8] L.J. Leon, F.A. Roberge, Directional characteristics of action potential propagation in cardiac muscle. A model study, Circ. Res. 69 (1991) 378–395.
[9] R.M. Shaw, Y. Rudy, Ionic mechanisms of propagation in cardiac tissue. Roles of the sodium and L-type calcium currents during reduced excitability and decreased gap junction coupling, Circ. Res. 81 (1997) 727–741.
[10] L. Romero, B. Trenor, J.M. Ferrero, C.F. Starmer, Non-uniform dispersion of the source-sink relationship alters wavefront curvature, PLoS One 8 (2013) e78328.
[11] P.M. Boyle, E.J. Vigmond, An intuitive safety factor for cardiac propagation, Biophys. J. 98 (2010) L57–L59.
[12] P.M. Boyle, W.H. Franceschi, M. Constantin, C. Hawks, T. Desplantez, N. A. Trayanova, et al., New insights on the cardiac safety factor: unraveling the relationship between conduction velocity and robustness of propagation, J. Mol. Cell. Cardiol. 128 (2019) 117–128.
[13] O.V. Aslanidi, P. Stewart, M.R. Boyett, H. Zhang, Optimal velocity and safety of discontinuous conduction through the heterogeneous Purkinje-ventricular junction, Biophys. J. 97 (2009) 20–39.
[14] Y. Wang, Y. Rudy, Action potential propagation in inhomogenous cardiac tissue: safety factor considerations and ionic mechanism, Am. J. Physiol. Heart Circ. Physiol. 278 (2000) H1019–H1029.
[15] L. Romero, B. Trenor, J.M. Ferrero, J. Saiz, A sensitivity study of the safety factor for conduction in the myocardium, Comput. Cardiol. 32 (2005) 873–876.
[16] L. Romero, B. Trenor, J.M. Alonso, C. Tobon, J. Saiz, J.M. Ferrero Jr., The relative role of refractoriness and source-sink relationship in reentry generation during simulated acute ischemia, Ann. Biomed. Eng. 37 (2009) 1560–1571.
[17] Z. Qu, Y. Xie, A. Garfinkel, J.N. Weiss, T-wave alternans and arrhythmogenesis in cardiac diseases, Front. Physiol. 1 (2010) 154.
[18] S. Rohr, B.M. Salzberg, Characterization of impulse propagation at the microscopic level across geometrically defined expansions of excitable tissue: multiple site optical recording of transmembrane voltage (MSORTV) in patterned growth heart cell cultures, J. Gen. Physiol. 104 (1994) 287–309.
[19] V.G. Fast, A.G. Kléber, Cardiac tissue geometry as a determinant of unidirectional conduction block: assessment of microscopic excitation spread by optical mapping in patterned cell cultures and in a computer model, Cardiovasc. Res. 29 (1995) 697–707.
[20] A.A. Kondratyev, J.G. Ponard, A. Munteanu, S. Rohr, J.P. Kucera, Dynamic changes of cardiac conduction during rapid pacing, Am. J. Physiol. Heart Circ. Physiol. 292 (2007). H1796–811.
[21] Q. Jin, K.Y. Lee, Z. Selimi, D. Shimura, E. Wang, J.F. Zimmerman, et al., Determinants of electrical propagation and propagation block in arrhythmogenic cardiomyopathy, J. Mol. Cell. Cardiol. 186 (2024) 71–80.
[22] C.H. Luo, Y. Rudy, A model of the ventricular cardiac action potential. Depolarization, repolarization, and their interaction, Circ. Res. 68 (1991) 1501–1526.
[23] Y. Prudat, J.P. Kucera, Nonlinear behaviour of conduction and block in cardiac tissue with heterogeneous expression of connexin 43, J. Mol. Cell. Cardiol. 76 (2014) 46–54.
[24] F. Jousset, A. Maguy, S. Rohr, J.P. Kucera, Myofibroblasts electrotonically coupled to cardiomyocytes alter conduction: insights at the cellular level from a detailed in silico tissue structure model, Front. Physiol. 7 (2016) 496.
[25] S.A. De Simone, S. Moyle, A. Buccarello, C. Dellenbach, J.P. Kucera, S. Rohr, The role of membrane capacitance in cardiac impulse conduction: an optogenetic study with non-excitable cells coupled to cardiomyocytes, Front. Physiol. 11 (2020) 194.
[26] Y. Prudat, R.V. Madhvani, M. Angelini, N.P. Borgstom, A. Garfinkel, H. S. Karagueuzian, et al., Stochastic pacing reveals the propensity to cardiac action potential alternans and uncovers its underlying dynamics, J. Physiol. 594 (2016) 2537–2553.
[27] P. Beauchamp, C. Choby, T. Desplantez, K. de Peyer, K. Green, K.A. Yamada, et al., Electrical propagation in synthetic ventricular myocyte strands from germline connexin 43 knockout mice, Circ. Res. 95 (2004) 170–178.
[28] A. Buccarello, M. Azzarito, F. Michoud, S.P. Lacour, J.P. Kucera, Uniaxial strain of cultured mouse and rat cardiomyocyte strands slows conduction more when its axis is parallel to impulse propagation than when it is perpendicular, Acta Physiol (Oxford) 223 (2018) e13026.
[29] S. Nayir, S.P. Lacour, J.P. Kucera, Active force generation contributes to the complexity of spontaneous activity and to the response to stretch of murine cardiomyocyte cultures, J. Physiol. 600 (2022) 3287–3312.
[30] S. Rohr, R. Flückiger-Labrada, J.P. Kucera, Photolithographically defined deposition of attachment factors as a versatile method for patterning the growth of different cell types in culture, Pflugers Arch. 446 (2003) 125–132.
[31] S.M. Shors, A.V. Sahakian, H.J. Sih, S. Swiryn, A method for determining high-resolution activation time delays in unipolar cardiac mapping, IEEE Trans. Biomed. Eng. 43 (1996) 1192–1196.
[32] S. Rohr, B.M. Salzberg, Multiple site optical recording of transmembrane voltage in patterned growth heart cell cultures: assessing electrical behavior, with microsecond resolution, on a cellular and subcellular scale, Biophys. J. 67 (1994) 1301–1315.
[33] J.N. Weiss, A. Karma, Y. Shiferaw, P.S. Chen, A. Garfinkel, Z. Qu, From pulsus to pulseless: the saga of cardiac alternans, Circ. Res. 98 (2006) 1244–1253.
[34] E. de Lange, J.P. Kucera, Alternans resonance and propagation block during supernormal conduction in cardiac tissue with decreased $[K^+]_o$, Biophys. J. 98 (2010) 1129–1138.
[35] M. Miragoli, G. Gaudesius, S. Rohr, Electrotonic modulation of cardiac impulse conduction by myofibroblasts, Circ. Res. 98 (2006) 801–810.
[36] P. Beauchamp, T. Desplantez, M.L. McCain, W. Li, A. Asimaki, G. Rigoli, et al., Electrical coupling and propagation in engineered ventricular myocardium with heterogeneous expression of connexin43, Circ. Res. 110 (2012) 1445–1453.
[37] E.D. Overholt, R.W. Joyner, R.D. Veenstra, D. Rawling, R. Wiedmann, Unidirectional block between Purkinje and ventricular layers of papillary muscles, Am. J. Physiol. Heart Circ. Physiol. 247 (1984) H584–H595.
[38] C. Cabo, A.M. Pertsov, W.T. Baxter, J.M. Davidenko, R.A. Gray, J. Jalife, Wave-front curvature as a cause of slow conduction and block in isolated cardiac muscle, Circ. Res. 75 (1994) 1014–1028.
[39] V.G. Fast, A.G. Kléber, Block of impulse propagation at an abrupt tissue expansion: evaluation of the critical strand diameter in 2- and 3-dimensional computer models, Cardiovasc. Res. 30 (1995) 449–459.
[40] P.M. Boyle, C.J. Park, H.J. Arevalo, E.J. Vigmond, N.A. Trayanova, Sodium current reduction unmasks a structure-dependent substrate for arrhythmogenesis in the normal ventricles, PLoS One 9 (2014) e86947.
[41] S. Rohr, J.P. Kucera, Involvement of the calcium inward current in cardiac impulse propagation: induction of unidirectional conduction block by nifedipine and reversal by bay K 8644, Biophys. J. 72 (1997) 754–766.
[42] H.J. Jongsma, H.E. van Rijn, Electrotonic spread of current in monolayer cultures of neonatal rat heart cells, J. Membr. Biol. 9 (1972) 341–360.
[43] K. Suga, H. Kato, S. Akita, T. Sakurai, R. Ota, T. Okada, et al., Optimal ablation settings of TactiFlex SE laser-cut irrigated-tip catheter: comparison with ThermoCool SmartTouch SurroundFlow porous irrigated-tip catheter, J. Interv. Card. Electrophysiol. (2024). Online ahead of print https://doi.org/10.1007/s10840-024-01797-9.
[44] M. Masuda, Y. Matsuda, H. Uematsu, M. Asai, S. Okamoto, T. Ishihara, et al., Atrial functional substrates for the prediction of atrial fibrillation recurrence after pulmonary vein isolation, Am. J. Cardiol. 218 (2024) 43–50.
[45] E. de Lange, J.P. Kucera, The transfer functions of cardiac tissue during stochastic pacing, Biophys. J. 96 (2009) 294–311.
[46] J.R. Padilla, R.D. Anderson, C. Joens, S. Masse, A. Bhaskaran, A. Niri, et al., Orientation of conduction velocity vectors on cardiac mapping surfaces, Europace 25 (2023) 1172–1182.
[47] P. Lee, J.G. Quintanilla, J.M. Alfonso-Almazan, C. Galan-Arriola, P. Yan, J. Sanchez-Gonzalez, et al., In vivo ratiometric optical mapping enables high-resolution cardiac electrophysiology in pig models, Cardiovasc. Res. 115 (2019) 1659–1671.
[48] C. O'Shea, A.P. Holmes, J. Winter, J. Correia, X. Ou, R. Dong, et al., Cardiac optogenetics and optical mapping - overcoming spectral congestion in all-optical cardiac electrophysiology, Front. Physiol. 10 (2019) 182.

Stochastic and alternating pacing paradigms to assess the stability of cardiac conduction

Stephan De Waard, Helene Hinnen and Jan P. Kucera

Department of Physiology, University of Bern, Bern, Switzerland

Supplementary material

Detailed Materials and methods

Modeling of conduction across expansions

Model of an expanding strand in 2 dimensions

Conduction was simulated in a 2-dimensional network of excitable elements arranged on a square lattice (Δx=Δy=60 μm). Unless specified otherwise, the network consisted of a 5-element wide and 50-element long strand merging into a 50-element by 101-element rectangular expansion, as illustrated in Figure 1A of the main article and as used in previous work [1]. Conduction from the strand into the expansion is characterized by a current-to-load mismatch, which predisposes to conduction block when the Na^+ current is decreased [2] or pacing rate is increased [1,3].

Model of the membrane ion currents

We used a modified version of the Luo-Rudy 1 model (LR1) [4] that was adjusted to replicate previous observations in small rodent cardiomyocyte cultures [1,5-7], as detailed below.

The original LR1 model consists of six currents that together define the total membrane ion current I_{ion}. These currents are the voltage-gated Na^+ current I_{Na}, the voltage-gated Ca^{2+} current I_{Ca}, (called slow inward current I_{si} by Luo and Rudy [4]), the time-dependent (voltage-gated) K^+ current I_K, the time-independent plateau current I_{Kp} (corresponding to the transient outward K^+ current), the inwardly rectifying K^+ current I_{K1}, and a background current I_b:

$$I_{ion} = I_{Na} + I_{Ca} + I_K + I_{Kp} + I_{K1} + I_b$$

These currents are expressed as current densities per cm^2 of membrane ($\mu A/cm^2$).

Na^+ current

I_{Na} was defined as in the original LR1 model as

$$I_{Na} = g_{Na} \cdot m^3 hj \cdot (V - E_{Na})$$

where g_{Na} is the maximum I_{Na} conductance, m is the activation gating variable, h is the rapid inactivation gating variable, j is the slow inactivation gating variable, V is the membrane potential and E_{Na} is the Nernst potential of Na^+:

$$E_{Na} = \frac{RT}{F} \ln\left(\frac{[Na^+]_e}{[Na^+]_i}\right)$$

with R being the gas constant, F the Faraday constant, and T the absolute temperature (310.15 K). $[Na^+]_e$ and $[Na^+]_i$ are the extracellular and intracellular Na^+ concentrations (140 and 18 mmol/L), respectively.

Compared to the original LR1 model, g_{Na} was reduced from 23 to 8.1 mS/cm^2 to calibrate the model for the conduction velocity (CV) and maximum rate of rise of the action potential upstroke observed in small rodent cardiomyocyte cultures, as described previously [5,6]. In addition, to account for similar pacing cycle lengths at which conduction starts to block across the expansion as observed in the experiments of the present study (around 120 ms), the rate constants of the slow inactivation gate j (functions α_j and β_j [4]) were increased twofold to decrease post-repolarization refractoriness.

Ca^{2+} current

I_{Ca} was defined as in the original LR1 model as

$$I_{Ca} = g_{Ca} \cdot df \cdot (V - E_{Ca})$$

where g_{Ca} is the maximum I_{Ca} conductance, d is the activation gating variable, f is the inactivation gating variable, and E_{Ca} is the reversal potential of I_{Ca}:

$$E_{Ca} = 7.7 - 13.0287 \cdot \ln([Ca^{2+}]_i)$$

with numeric values in mV, and intracellular Ca^{2+} concentration $[Ca^{2+}]_i$ in mmol/L. E_{Ca} corresponds to an extracellular Ca^{2+} concentration of 1.8 mmol/L.

In the original LR1 model, I_{Ca} is of small magnitude and its kinetics are very slow. Because I_{Ca} can contribute to support propagation in a situation of current-to-load

mismatch once I_{Na} is inactivated [2], g_{Ca} was increased from 0.09 to 0.18 mS/cm^2 and the kinetics of the d and f gates were accelerated [5,6]. In the present work, the original LR1 gating functions α_d and β_d were increased by a factor 60 and the functions α_f and β_f by a factor 4, respectively. Finally, as previously described [6], the gating functions α_d and β_d were shifted by 6 mV towards more positive potentials to avoid spontaneous activity caused by the I_{Ca} window current in presence of a reduced I_{K1} (see below). The formulation for the dynamic changes of $[Ca^{2+}]_i$ was identical to that in the original LR1 model.

Voltage gated (time-dependent) K^+ current

I_K was defined as in the original LR1 model as

$$I_K = g_K \cdot x \cdot x_i \cdot (V - E_K)$$

where g_K is the maximum I_K conductance, x is the activation gating variable, x_i is the time-independent inactivation gating variable (function of V only), and E_K is the reversal potential of I_K:

$$E_K = \frac{RT}{F} \ln\left(\frac{[K^+]_e + PR_{NaK} \cdot [Na^+]_e}{[K^+]_i + PR_{NaK} \cdot [Na^+]_i}\right)$$

with $[K^+]_e$ and $[K^+]_i$ being the extracellular and intracellular K^+ concentrations (5.4 and 145 mmol/L, respectively), and PR_{NaK} being the Na^+/K^+ permeability ratio [4].

The original LR1 model was developed based on guinea-pig ventricular myocyte data. However, in small rodents, the cardiac action potential is considerably shorter. Therefore, g_K was increased, as formerly described [5,6]. In the present work, g_K was increased from 0.282 (original nominal value at $[K^+]_e$=5.4 mmol/L) to 1.5 mS/cm^2. In addition, the kinetics of I_K were accelerated by multiplying the gating functions α_x and β_x of the original LR1 model by a factor 2 to further shorten the action potential in consistency with our cultures in vitro, which can be paced at cycle lengths of 100 ms or even less.

Plateau K^+ current

The I_{Kp} formulation was identical to that of the original LR1 model.

Inward rectifier K^+ current

In the process of optimizing the model to simulate conduction in cultures of small rodent ventricular myocytes, we observed that the current-voltage relationship measured in such myocytes using patch-clamp was considerably less steep near resting membrane potential compared to the current-voltage relationship of the original

LR1 model, indicating that I_{K1} is smaller in the cultured myocytes [6]. Therefore, as in this previous study [6], we replaced the I_{K1} formulation of Luo and Rudy by that proposed by Korhonen et al. [8]:

$$I_{K1} = g_{K1} \cdot \frac{[K^+]_e}{[K^+]_e + 0.210} \cdot \frac{V - E_{K1} - 6.1373}{0.1653 + e^{0.0319(V - E_K - 6.1373)}}$$

where g_{K1} is 0.0515 mS/cm^2 and E_{K1} is the Nernst potential of K^+.

Background current

In the modified LR1 model, in presence of the reduced I_{K1}, the background current I_b led to an unstable resting membrane potential and spontaneous activity. I_b was therefore set to 0.

Model of capacitive and resistive properties

Specific membrane capacitance c_m was 1 µF/cm^2. The capacitance C of the excitable elements was defined as $R_{area} \cdot \Delta x \cdot \Delta y \cdot c_m$, where R_{area} is a unitless factor (area ratio) of 2.4 accounting for the fact that in monolayer cultures, cardiomyocytes exhibit a membrane both on their top and their bottom sides, and that the cultured cells overlap laterally to some extent [6]. C thus amounted to 86.4 pF for all excitable elements. Myoplasmic resistance was determined based on a myoplasmic resistivity of 124 Ω·cm and a cell thickness of 3 µm [6]. Gap junctional resistance was based on a resistance per length of cell-cell contact of 77.4 nS/µm, as derived in Jousset et al. [6]. As myoplasmic and gap junctional resistances are in series, lumped resistance between adjacent excitable elements was computed as the sum of both and amounted to 0.6287 MΩ, corresponding to a conductance G between elements of 1.5907 µS. The value of G was uniform and identical in both x and y directions (isotropic tissue).

Applying Kirchhoff's current law for every excitable element yields the following equation for the rate of change of V (this equation is equivalent to that obtained with a finite-difference scheme and Neumann boundary conditions):

$$\frac{dV}{dt} = -\frac{I_{ion} + I_{stim}}{c_m} + \frac{1}{C} \sum_{i \in Neighbors} G \cdot (V_i - V)$$

where I_{stim} is the stimulation current density injected into stimulated elements (see "Pacing protocols" below) and 0 otherwise. V_i are the membrane potentials of the neighboring elements (2, 3 or 4 elements, depending on position in the computational domain). C and G correspond together to an isotropic diffusion coefficient $G/(R_{area} \cdot c_m)$ of $6.63 \cdot 10^{-4}$ cm^2/ms.

Conduction velocity (CV) at a pacing cycle length of 200 ms in the center of a non-expanding 5-element wide and 100-element long strand strand was 38.7 cm/s, comparable to CVs observed in cardiomyocyte cultures [1,5,6].

Pacing protocols

The model tissue was paced by injecting a suprathreshold 2 ms current pulse (–150 $\mu A/cm^2$) into the first column of excitable elements at the extremity of the strand (see Figure 1A of the main article). For simulations of retrograde conduction, this current was injected into the last column of elements along the right edge of the network. Antegrade conduction stability from the strand into the expansion was challenged in a regulated fashion by gradually decreasing pacing cycle length (CL) in a downward ramp. In this manner, the action potentials (APs) were elicited progressively within the relative refractory period, during which the recovery of I_{Na} is incomplete. In further simulations, retrograde conduction was investigated by pacing the computational domain along its right edge. Three different types of protocols were designed and compared regarding their ability to reveal pronounced local variations of conduction and to pinpoint sites of unstable conduction particularly susceptible to block. Similar pacing protocols were used in the in vitro experiments (see below).

Ramp protocol without variations: The cardiac tissue underwent a short period (6 s) of initial pacing at a predefined basic cycle length (200-250 ms) to allow reaching steady state. Subsequently, the CL was progressively decreased (see Figure 1B of the main article, top left panel) on a beat-to-beat basis to 80-100 ms over several minutes, which led to the occurrence of conduction block at the expansion site. To avoid a too rapid decrease of CLs as the relative refractory period is approached, the descending CL ramps were constructed such that the instantaneous pacing rate (1/CL) rather than CL itself changed linearly with time (Figure 1B of the main article, bottom left panel), as done previously [9].

Ramp protocol with stochastic variations: A sequence of pacing CLs was constructed as described above. Then, every CL was perturbed by adding a random number drawn from a Gaussian distribution with a mean of zero and a standard deviation (SD) of either 2 or 5 ms. In such a protocol, the applied perturbations continuously reinforce each other through CV restitution [10] and AP duration (APD) restitution [9,10].

Ramp protocol with alternating variations: Instead of incorporating stochastic variations into the CL ramp protocol, the even terms of the CL series without variations were lengthened by 2 or 5 ms and the odd terms were shortened by the same amount. This protocol was based on our previous observation that pacing with alternating CL variations may maximize conduction disturbances arising from tissue heterogeneities [11].

Numerical methods

The simulations were conducted using a constant time step of 0.005 ms. Gating variables were integrated using the method of Rush and Larsen [12] while intracellular Ca^{2+} concentration and membrane potential were integrated using the forward Euler method. Membrane potential was registered at 10 locations evenly spaced (300 μm) along the axis of the strand, 5 before and 5 after the expansion, as illustrated in Figure

1A of the main article. Activation time was defined at these locations as the moment when membrane potential passed –35 mV during depolarization. These activation times were used to calculate the successive conduction times (CTs) between adjacent recording locations. These CTs were subsequently analyzed in a similar manner as for the in vitro experiments to compute metrics assessing conduction stability (see "Metrics to assess conduction instability" below). Conduction block was identified as the absence of passing the –35 mV threshold in the distal part of the expansion, as previously [1,6]. APD was determined at repolarization to –75 mV. All simulations were run in MATLAB (version R2019a, MathWorks).

Experiments in patterned cardiomyocyte cultures grown on microelectrode arrays

Ethical approval

All animal handling procedures adhered strictly to the ethical principles and guidelines set forth by the Swiss Academy of Medical Sciences. The acquisition, care, and experimental procedures involving animals complied with the European Convention for the Protection of Vertebrate Animals used for Experimental and other Scientific Purposes. The protocols underwent review and approval by the Commission of Animal Experimentation of the Cantonal Veterinary Office of the Canton of Bern, Switzerland (authorization no. BE115/2022), in accordance with Swiss legislation. Experimental activities were conducted following the directives outlined by the animal welfare committee of the University of Bern.

Isolation of neonatal mouse ventricular cells

Myocyte cultures derived from neonatal (0-1 day postpartum) or fetal (19.5 days postcoitum) wild-type C57BL/6J mice (Charles River) were prepared following protocols detailed in previous publications [5,13-15]. The animals were provided ad libitum access to food and water. Neonates were euthanized via decapitation, while fetal specimens were obtained by terminating anesthesia in the mother animal through intraperitoneal injection of xylazine and ketamine (10 and 80 mg/kg body mass, respectively). After confirming the loss of pedal reflex, decapitation was performed, and the uterus was extracted to collect the fetuses, which were then euthanized via decapitation.

In brief, upon extraction of the hearts, ventricles were minced into 1 mm pieces. The cardiomyocytes were enzymatically dissociated using trypsin (0.075%; Gibco) and pancreatin (100 mg/L; Sigma-Aldrich) in Hanks' balanced salt solution without Ca^{2+} and Mg^{2+} (HBSS; Bioconcept) supplemented with phenol red at 35°C. Regardless of the animals' sex, all cells were pooled together. The resulting cell suspension underwent centrifugation, followed by resuspension in enzyme-free culture medium and pre-plating for 2 hours to reduce myofibroblast content. Subsequently, cell counting was performed using a Neubauer chamber (Bioswisstech).

Patterned cultures on microelectrode arrays

The isolated ventricular cells were directly seeded on microelectrode arrays (MEAs) that were microfabricated (Campus Biotech, Geneva, Switzerland) on borosilicate glass according to our specifications and mounted in custom-fabricated culture chambers [3]. The MEAs incorporated four rows of 12 transparent indium-tin oxide electrodes (diameter: 40 µm; interelectrode spacing: 0.5 mm) with a platinized stimulation dipole at each end (Figure 1C of the main article). Over these rows of electrodes, cardiomyocyte strands (width: 100-150 µm) expanding abruptly into rectangular expansions were prepared using previously described photolithographic techniques [16]. Briefly, MEAs were spin-coated with negative photoresist and the desired patterns were transferred by exposure to ultraviolet light through negative masks. The exposed substrates were subsequently developed using xylol, thus leaving photoresist-free regions. These regions were coated with type I collagen (from rat tail, Sigma-Aldrich). Substrates were then incubated in bi-distilled water at 36°C for ~1h causing the photoresist to soften, allowing for its stripping with a fine forceps. Finally, the substrates were sterilized using ultraviolet light.

The myocytes were seeded at a density of 4.4×10^5 cells/cm^2. The patterned myocyte cultures were maintained in medium 199 with Hanks' salts (Sigma-Aldrich) supplemented with 10% neonatal calf serum (Amimed), 10 mmol/L HEPES (Gibco), 0.68 mmol/L L-glutamine (Sigma-Aldrich), 20 mg/L streptomycin and 20000 U/L penicillin (Bioswisstech) to prevent bacterial proliferation and 100 mmol/L bromodeoxyuridine (Sigma Aldrich) to minimize fibroblast proliferation. The preparations were incubated at 36°C and 0.9% CO_2 for 2-3 days prior to experiments. Medium exchange (containing 5% neonatal calf serum) and removal of non-attached cells was performed on the first day after seeding. A schematic and a microphotograph of a preparation is shown in Figure 1D of the main article.

Electrophysiological recordings

To ensure uniformity in the extracellular environment across all preparations during electrophysiological recordings, the culture medium was replaced with HBSS (Gibco), in accordance with previous work [2,3,5]. Subsequently, the chambers, which incorporated a connection interface, were linked to a customized amplifier array (with a gain of 1000x) and stimulator, and replaced into the incubator (36°C). Electrophysiological procedures started following an equilibration period of approximately 60 minutes.

The preparations were stimulated using biphasic voltage pulses of opposite polarity (amplitude: 0.7-1.5 V, duration of each phase: 1 ms). Pacing protocols similar to those used in the simulations were used. For every strand investigated, a ramp protocol without variations, two ramp protocols with stochastic CL variations (SD of 2 ms and 5 ms) and two ramp protocols with alternating CL variations (±2 ms and ±5 ms) were conducted (see Figure 1B of the main article). Only preparations demonstrating continuous 1:1 stimulus capture (before block eventually occurred at the expansion site) were used for further analysis. Extracellular unipolar electrograms were recorded from the corresponding row of 12 microelectrodes and sampled at 10 kHz.

Data analysis: metrics to assess conduction instability

Conduction times in the experimental recordings

In a first step, the electrograms were high-pass filtered using a digital AC coupling filter (time constant: 1 ms) to minimize the capacitive transients consecutive to the stimulation artifacts. Activation times were then identified at the occurrence of the minimum of the first derivative (computed using the central difference method) of the extracellular signals [3,5]. All electrograms in all recordings were curated by visual inspection using a custom-designed graphic user interface to ensure that all activations were detected properly. In the case of slow or noisy signals, the electrograms were low-pass filtered using a phase-preserving Gaussian convolution kernel.

Finding the minimum of the derivative using this scheme rounds the activation time to its next integer multiple of the sampling period (0.1 ms). As a consequence, calculating conduction times (CTs) between adjacent electrodes as the difference between activation times results in quantized values and produce jitter, which overestimates the variability of CT. To circumvent this problem, we used in a second step the algorithm of Shors et al. [17] to compute the CTs. Accordingly, we computed the CTs between adjacent electrode pairs by finding the interpolated time of the negative-to-positive zero crossing of the Hilbert transform of the cross-correlation function of the derivatives of the two electrograms [17]. In practice, we applied this algorithm on 3-ms windows centered on the activation times identified by the minima of the derivatives [17].

This algorithm is resilient to noise and provides accurate and stable results [17]. In our setting, in the case of stable conduction (at long pacing CLs) inside cardiomyocyte strands, it reduced the standard deviation of CTs to less than 0.005 ms, which is about 5% of the sampling period. The accuracy of this algorithm comes at the expense of not providing the activation times at the two electrodes but only their difference. Nevertheless, this was not a limitation because our analysis focused on the variability of CTs (see below). However, this algorithm is sensitive to capacitive transients that typically extend over a few ms after stimulation. Therefore, in all analyses, the signals from the two electrodes most proximal to the stimulation site were not considered, leaving 10 electrodes with 9 equally spaced intervals.

This analysis was conducted until the first occurrence of block at the expansion site (confirmed by visual inspection of the signals). In one experiment, one of the channels (corresponding to an electrode located on the side of the strand) was poorly connected and not utilizable; in this case, the CT from the previous electrode and the next electrode was halved and used as interpolated CT.

Conduction velocity in the strand before the expansion

In the experiments, CV was assessed in the proximal part of the preparation (before the expansion) by linear regression of activation time vs. position. In simulations, CV was assessed in the center of a non-expanding strand (300 μm wide, 6 mm long).

Metrics to assess conduction stability

In simulations and in experiments, for every interval between adjacent recording locations, we computed the standard deviation and the amplitude of alternating variations of CT in a sliding window of 10 consecutive APs, as follows. First, the sequence of 10 consecutive values was detrended using a second-degree polynomial.

Standard deviation of conduction times, SD(CT): To examine the variability of conduction during ramps with stochastic variations, we computed the standard deviation of this detrended set.

Alternation amplitude of conduction times, AA(CT): To examine the variability of conduction during ramps with alternating variations, we computed the alternation amplitude of CT as the absolute difference between the mean of the odd values and the mean of the even values within the detrended set.

As SD(CT) and AA(CT) are larger for intervals in which conduction is unstable, the time progressions of these two metrics were examined as markers to predict the site of block.

Metrics to predict the site of block in experiments

To evaluate the ability of SD(CT) and AA(CT) to localize sites of conduction prone to block, their corresponding values were considered as distributions over the interelectrode intervals, and their first two moments were calculated.

Specifically, the first moment (corresponding to the location of the mean of the distribution) was calculated as

$$M_1 = \frac{\sum_{i=1}^{N} m_i \cdot i}{\sum_{i=1}^{N} m_i},$$

where N is the number of spatial intervals (numbered sequentially from 1 to N, with N=9 as we considered 10 equally spaced electrodes), i is the index of the interval and m_i is the considered metric (SD(CT) or AA(CT)).

The square root M_2 of the second moment (centered on M_1, corresponding to the standard deviation of the distribution) was calculated as

$$M_2 = \sqrt{\frac{\sum_{i=1}^{N} m_i \cdot (i - M_1)^2}{\sum_{i=1}^{N} m_i}}.$$

M_1 thus provides an estimate of the site of block and M_2 is a measure of the accuracy of this estimation. All analyses were done using MATLAB.

Safety factor in computer simulations

In selected simulations, the safety factor (SF) was computed according to the SF_{m2} formulation by Romero et al., as detailed in their publication [18]. This formulation is inspired by the work of Shaw and Rudy, which was initially developed for conduction in 1-dimensional cell strands [19]. The SF_{m2} formulation builds upon that of Shaw and Rudy and compensates partially the artefactual dependence of the SF on the direction of propagation relative to the discretization lattice used in 2-dimensional models (for details, see Romero et al. [18]).

Supplemental Figures

Supplemental Figure S1

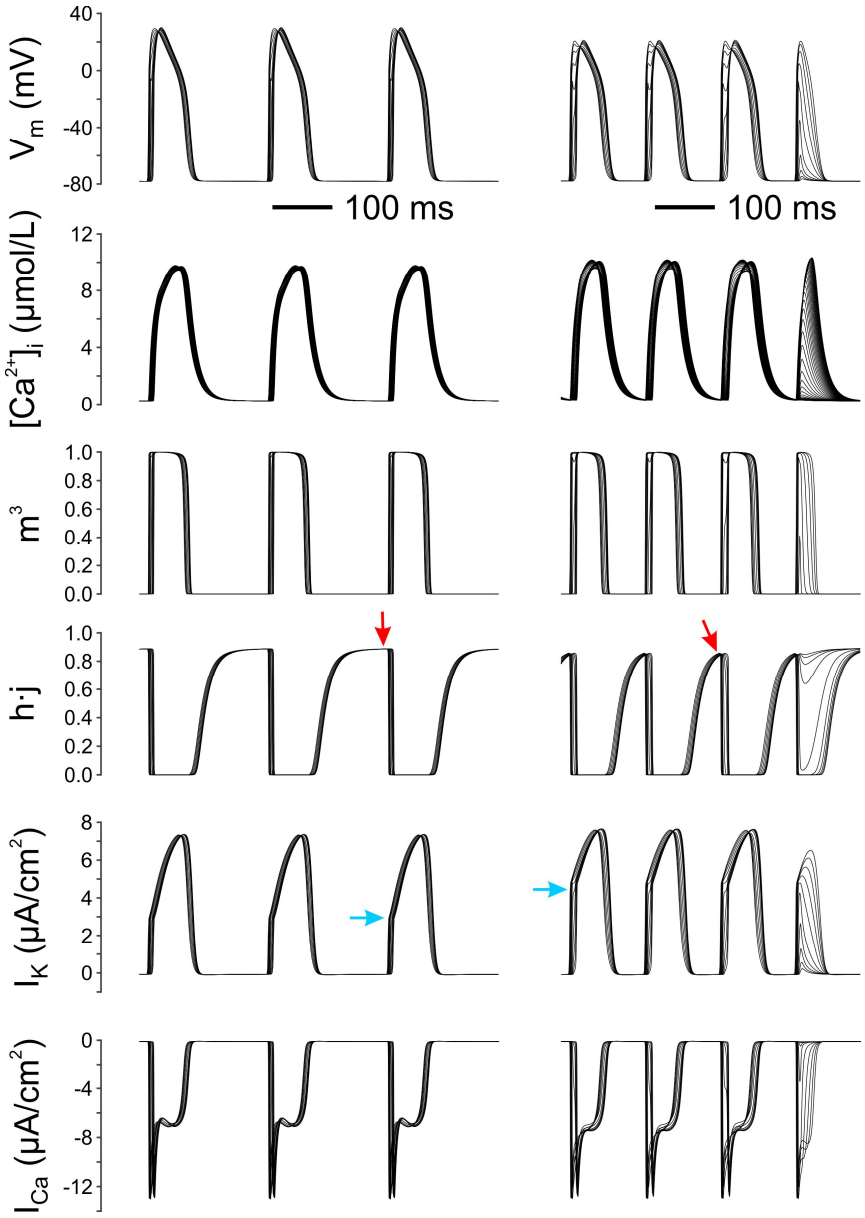

Supplemental Figure S1: Variables of the modified Luo-Rudy model during simulations of conduction across a tissue expansion. V_m: membrane potential; $[Ca^{2+}]_i$: intracellular calcium concentration; m^3: product of the three activation gates of the sodium current; h·j: product of the fast (h) and slow (j) inactivation gates of the sodium current, reflecting the availability of sodium channels; I_K: time-dependent potassium current; I_{Ca}: slow inward calcium current. Data are plotted for the 10 sites shown in Figure 2A of the main article for the ramp protocol without variations (same simulation as in Figure 2C). Left: successfully propagated APs at the beginning of the protocol (CL=200 ms). Right: Last 3 propagated APs and first AP blocked at the expansion (CL near 126 ms). Just before block, the AP was elicited in the relative refractory period (steeper recovery of sodium current availability h·j, red arrows), making the current-to-load mismatch more sensitive to CL variations. Note that at reduced CL, more potassium current is available immediately at the onset of the APs (less I_K deactivation, blue arrows), contributing to AP shortening. The calcium current and the calcium transients are similar in amplitude.

Supplemental Figure S2

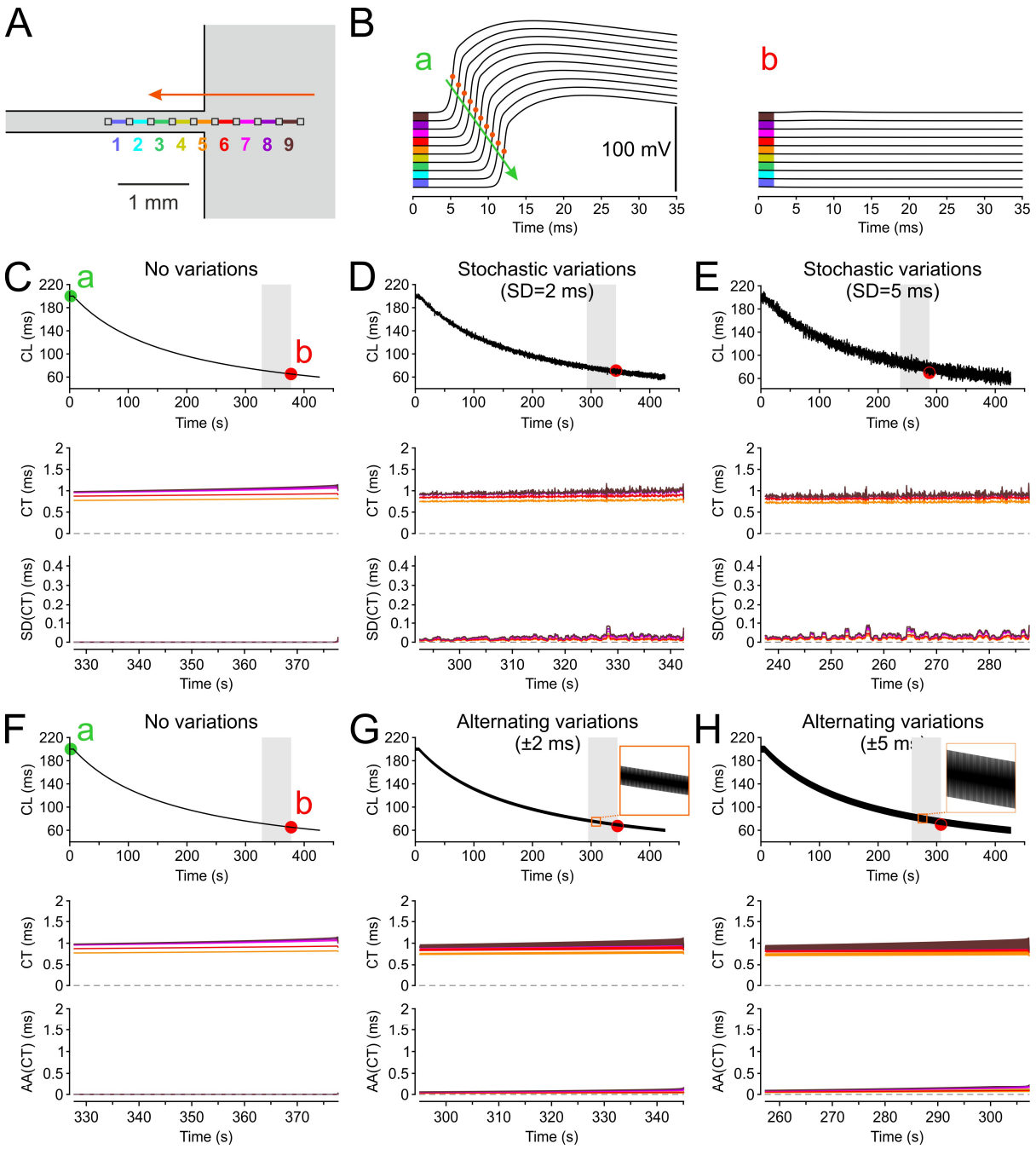

Supplemental Figure S2: Simulations of retrograde conduction variability across a tissue expansion. A: Schematic of the computational domain, with numbered and color-coded intervals between recording sites. The domain was stimulated along its right edge. Note the backwards orange arrow depicting the retrograde conduction direction from the rectangular expansion to the strand. B: Membrane potentials at the sites marked in A for a successfully propagated impulse at the beginning of a control pacing ramp (a, green arrow) and for the first stimulus that failed to generate a propagated AP (b, red arrow). Color coding as in A. The orange dots indicate the threshold of –35 mV defining activation time. C: Top: Ramp protocol without variations. The green and red markers correspond to the upstrokes shown in B. Middle and bottom: CT and SD(CT) during the last 50 s before the first stimulus that failed to elicit an AP (gray background in the ramp protocol). Labeling and color-coding as in A. D and E: Same as C, but for a ramp protocol with stochastic CL variations having a SD of 2 ms and 5 ms, respectively. The red markers indicate the first impulses that failed to elicit a propagated AP. F: Top: Ramp protocol without variations (as in C). Middle and bottom: CT and AA(CT) during the last 50 s before the first stimulus that failed to elicit an AP (gray background in the ramp protocol). G and H: Same as F, but for a ramp protocol with alternating CL variations of ±2 ms and ±5 ms, respectively. The red markers indicate the first impulses that failed to propagate. Noteworthy, compared to antegrade propagation (Figure 2 of the main article), retrograde propagation was characterized by only a minor disturbance in AP upstroke morphology and no structure-induced conduction block. Moreover, CTs were slightly shorter for intervals 6 and 7 compared to the other intervals, and, with time, there was no manifest increase of SD(CT) or AA(CT), which both remained very low.

Supplemental Figure S3: Rate-dependent evolution of local conduction times during propagation across a tissue expansion, in simulations (A, B) and in experiments (C to J), during ramp pacing protocols without CL variations. A: Schematic of the computational domain, with color-coded intervals between recording sites. B. Sliding mean CT vs. sliding mean CL (window of 10 beats) throughout the simulation until the occurrence of conduction block. Color coding as in A. C: Schematic of the experimental preparations showing the recording sites and the corresponding color-coded intervals used to investigate local CTs. D-J: Sliding mean CT vs. sliding mean CL (window of 10 beats) throughout the individual experiments (preparations 1 to 7), until the occurrence of conduction block. Color coding as in C. Note the typical increase of CT at and just after the expansion as CL is decreased, caused by the enhanced CV restitution due to the current to-load mismatch.

Supplemental Figure S3

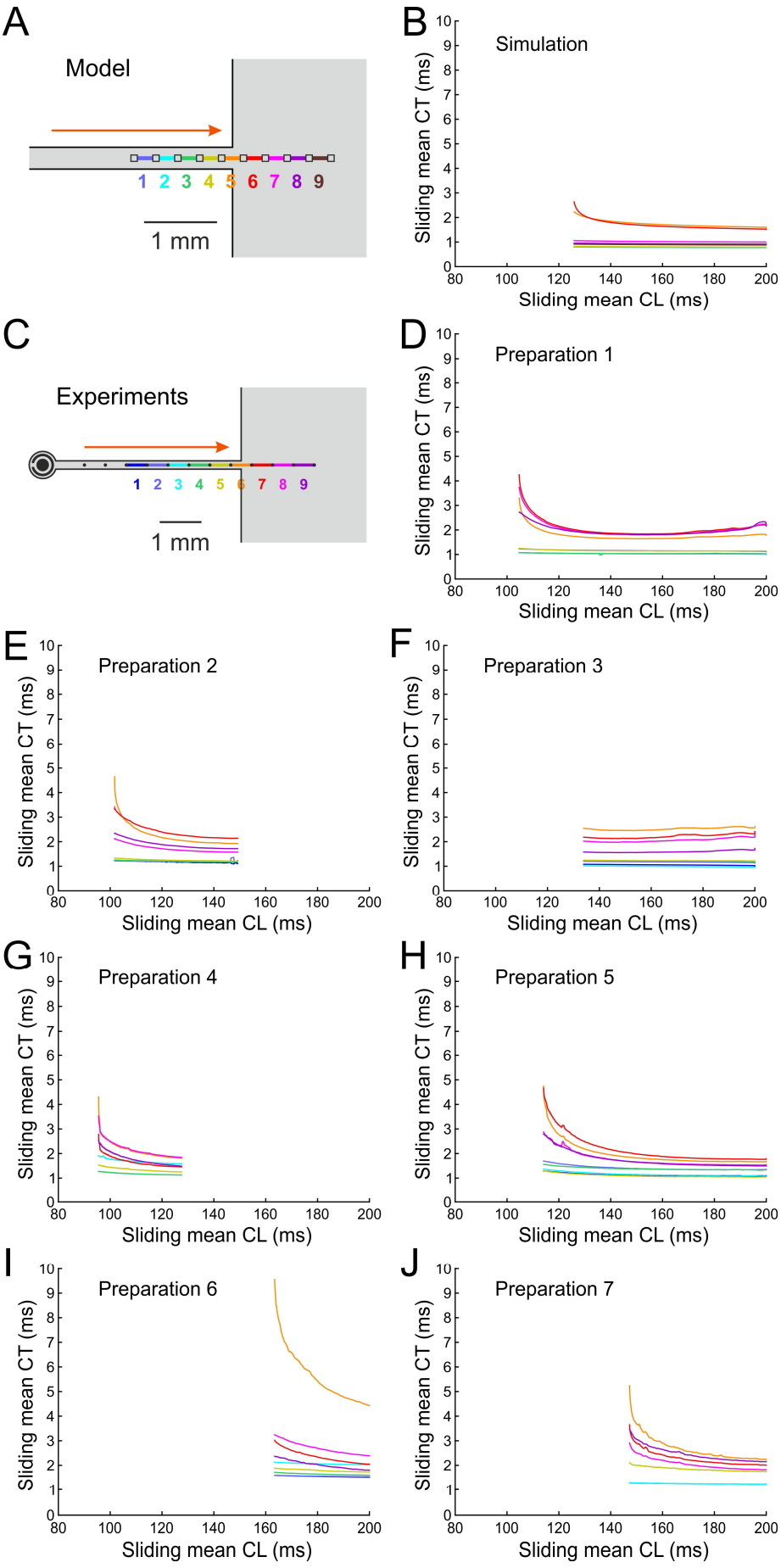

Supplemental Figure S4

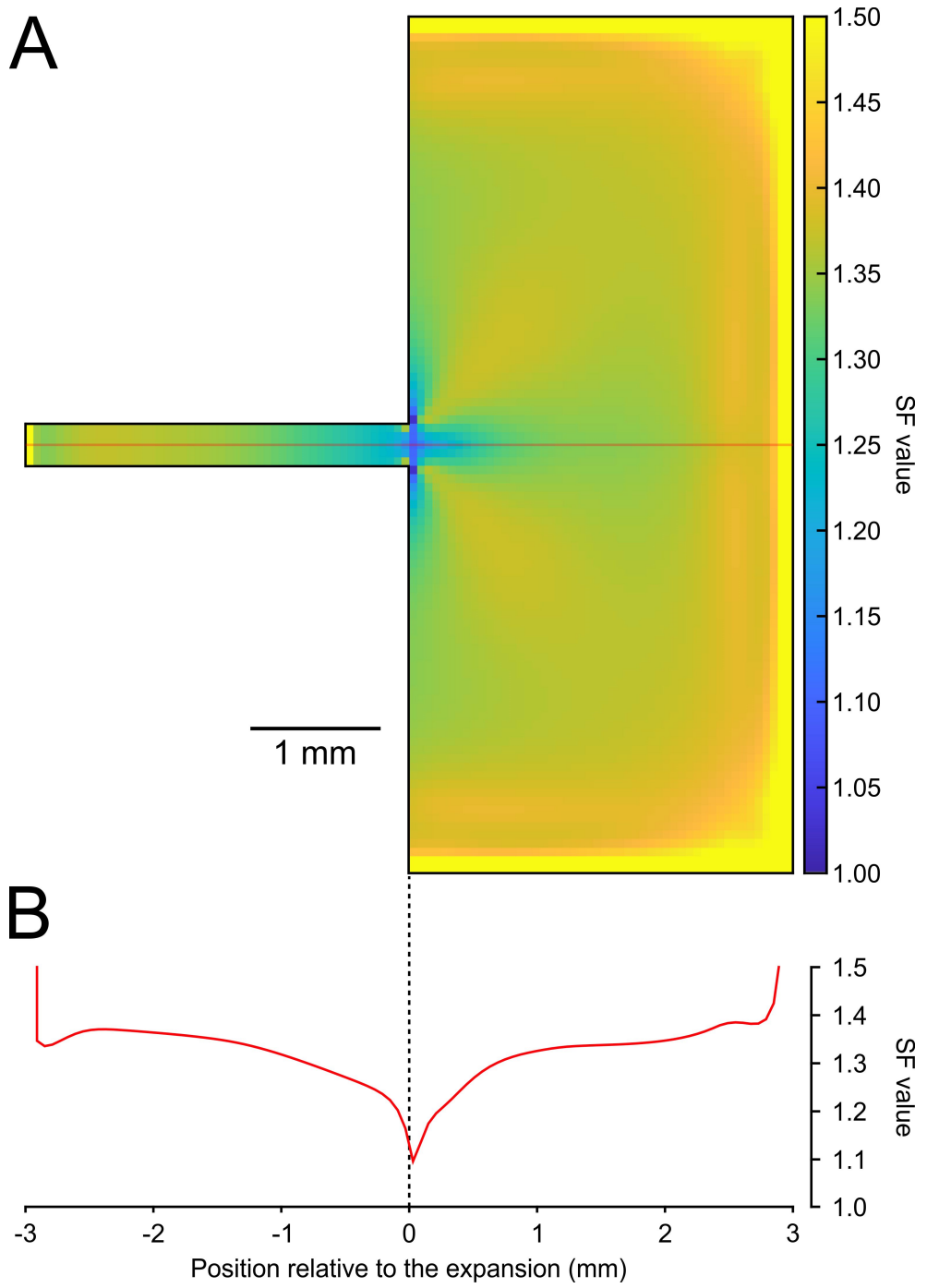

Supplemental Figure S4: Safety factor during antegrade AP propagation across a simulated tissue expansion. A: Schematic of the computational domain showing a color map of the SF during successful antegrade AP propagation. The analysis was conducted for the 30th AP elicited at a pacing CL of 200 ms at the beginning of a ramp protocol without variations. The SF was computed according to the SF_{m2} formulation by Romero et al. [18]. The transparent horizontal red line represents the axis of the expansion, for which the SF is also shown in B. B: SF profile along the axis of the expansion (red line depicted in A). The SF was decreased both before and after the expansion, and the minimum occurred in the first column of excitable elements inside the expansion.

Supplemental Figure S5

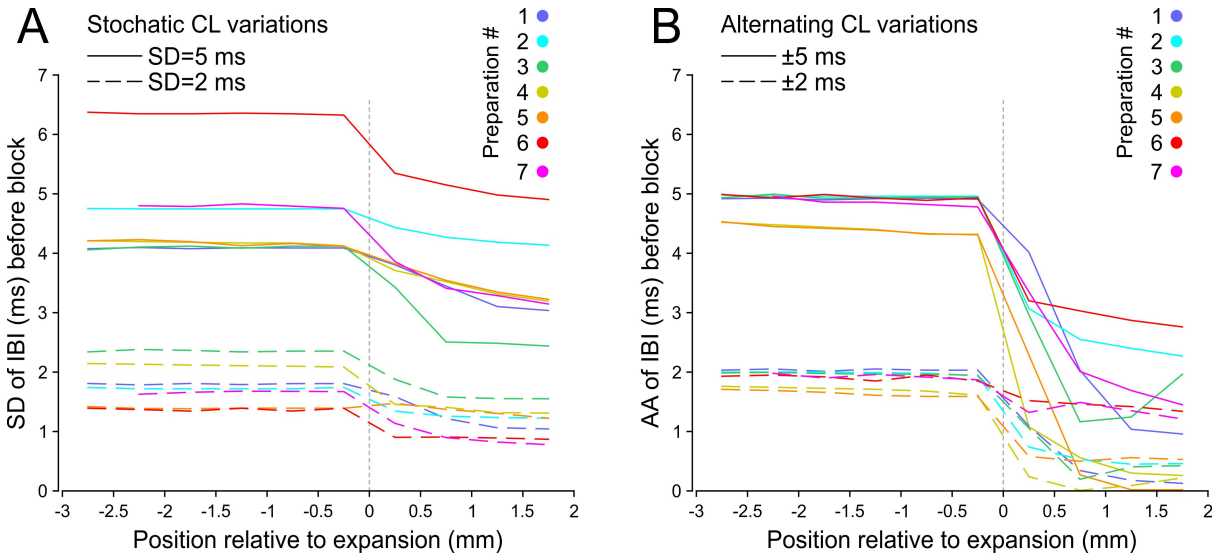

Supplemental Figure S5: Interbeat interval variability in the cultured expansions during stochastic and alternating pacing. A: Standard deviation (SD) of the last 10 IBIs before block occurred at the expansion vs. position along the preparation axis during ramp pacing protocols with stochastic pacing CL variations with a SD of 5 ms (solid lines) and 2 ms (dashed lines). The IBIs were computed at every recording electrode as the difference series of activation times, and hence reflect the CL variations introduced into the pacing protocol. Data from each individual preparation are plotted in a different color (legend). B: Same as A, but showing the alternation amplitude (AA) of the last 10 IBIs before block for ramp pacing protocols with alternating CL variations of ±5 ms (solid lines) and ±2 ms (dashed lines). Of note, although the SD and the AA of IBI became smaller after the expansion, they remained in most cases still sufficient to permit the detection of another site of vulnerable conduction further downstream, especially for pacing protocols with stochastic SD=5 ms or alternating ±5 ms CL variations.

References

[1] Jin Q, Lee KY, Selimi Z, Shimura D, Wang E, Zimmerman JF, et al. Determinants of electrical propagation and propagation block in arrhythmogenic cardiomyopathy. J Mol Cell Cardiol 2024; 186: 71-80.

[2] Rohr S, Kucera JP. Involvement of the calcium inward current in cardiac impulse propagation: induction of unidirectional conduction block by nifedipine and reversal by Bay K 8644. Biophys J 1997; 72: 754-66.

[3] Kondratyev AA, Ponard JG, Munteanu A, Rohr S, Kucera JP. Dynamic changes of cardiac conduction during rapid pacing. Am J Physiol Heart Circ Physiol 2007; 292: H1796-811.

[4] Luo CH, Rudy Y. A model of the ventricular cardiac action potential. Depolarization, repolarization, and their interaction. Circ Res 1991; 68: 1501-26.

[5] Prudat Y, Kucera JP. Nonlinear behaviour of conduction and block in cardiac tissue with heterogeneous expression of connexin 43. J Mol Cell Cardiol 2014; 76: 46-54.

[6] Jousset F, Maguy A, Rohr S, Kucera JP. Myofibroblasts electrotonically coupled to cardiomyocytes alter conduction: insights at the cellular level from a detailed in silico tissue structure model. Front Physiol 2016; 7: 496.

[7] De Simone SA, Moyle S, Buccarello A, Dellenbach C, Kucera JP, Rohr S. The role of membrane capacitance in cardiac impulse conduction: an optogenetic study with non-excitable cells coupled to cardiomyocytes. Front Physiol 2020; 11: 194.

[8] Korhonen T, Hanninen SL, Tavi P. Model of excitation-contraction coupling of rat neonatal ventricular myocytes. Biophys J 2009; 96: 1189-209.

[9] Prudat Y, Madhvani RV, Angelini M, Borgstom NP, Garfinkel A, Karagueuzian HS, et al. Stochastic pacing reveals the propensity to cardiac action potential alternans and uncovers its underlying dynamics. J Physiol 2016; 594: 2537-53.

[10] de Lange E, Kucera JP. The transfer functions of cardiac tissue during stochastic pacing. Biophys J 2009; 96: 294-311.

[11] de Lange E, Kucera JP. Alternans resonance and propagation block during supernormal conduction in cardiac tissue with decreased $[K^+]_o$. Biophys J 2010; 98: 1129-38.

[12] Rush S, Larsen H. A practical algorithm for solving dynamic membrane equations. IEEE Trans Biomed Eng 1978; 25: 389-92.

[13] Beauchamp P, Choby C, Desplantez T, de Peyer K, Green K, Yamada KA, et al. Electrical propagation in synthetic ventricular myocyte strands from germline connexin 43 knockout mice. Circ Res 2004; 95: 170-8.

[14] Buccarello A, Azzarito M, Michoud F, Lacour SP, Kucera JP. Uniaxial strain of cultured mouse and rat cardiomyocyte strands slows conduction more when its axis is parallel to impulse propagation than when it is perpendicular. Acta Physiol (Oxf) 2018; 223: e13026.

[15] Nayir S, Lacour SP, Kucera JP. Active force generation contributes to the complexity of spontaneous activity and to the response to stretch of murine cardiomyocyte cultures. J Physiol 2022; 600: 3287-312.

[16] Rohr S, Flückiger-Labrada R, Kucera JP. Photolithographically defined deposition of attachment factors as a versatile method for patterning the growth of different cell types in culture. Pflugers Arch 2003; 446: 125-32.

[17] Shors SM, Sahakian AV, Sih HJ, Swiryn S. A method for determining high-resolution activation time delays in unipolar cardiac mapping. IEEE Trans Biomed Eng 1996; 43: 1192-6.

[18] Romero L, Trenor B, Ferrero JM, Starmer CF. Non-uniform dispersion of the source-sink relationship alters wavefront curvature. PLoS One 2013; 8: e78328.

[19] Shaw RM, Rudy Y. Ionic mechanisms of propagation in cardiac tissue. Roles of the sodium and L-type calcium currents during reduced excitability and decreased gap junction coupling. Circ Res 1997; 81: 727-41.